Biomaterials 271 (2021) 120760

Contents lists available at ScienceDirect

Biomaterials

journal homepage: www.elsevier.com/locate/biomaterials

Development of an antibody-like T-cell engager based on VH-VL heterodimer formation and its application in cancer therapy

Seil Jang [a,b,f], Jaeho Song [b], NaYoung Kim [b], Jeonghyeon Bak [b], Keehoon Jung [c], Young Woo Park [b], Bum-Chan Park [b,**], Ho Min Kim [a,d,e,*]

[a] Biomedical Science and Engineering Interdisciplinary Program, Korea Advanced Institute of Science and Technology (KAIST), Daejeon, 34141, South Korea
[b] Y-BIOLOGICS, Inc., 17 Techno 4-ro, Yuseong-gu, Daejeon, 34013, South Korea
[c] Seoul National University College of Medicine, Seoul, 03080, South Korea
[d] Graduate School of Medical Science & Engineering, Korea Advanced Institute of Science and Technology (KAIST), 291 Daehak-ro, Yuseong-gu, Daejeon, 34141, South Korea
[e] Center for Biomolecular & Cellular Structure, Institute for Basic Science (IBS), Daejeon, 34126, South Korea
[f] CTCELLS, Inc., R7, 333 Techno Jungang-daero, Hyeonpung-eup, Dalseong-gun, Daegu, 42988, South Korea

ARTICLE INFO

Keywords:
Antibody-engineering
Bispecific antibody
T-cell engager
Cancer immunotherapy

ABSTRACT

Following the clinical success of immunotherapeutic antibodies, bispecific antibodies for cytotoxic effector cell redirection, tumor-targeted immunomodulation and dual immunomodulation, have received particular attentions. Here, we developed a novel bispecific antibody platform, termed Antibody-Like Cell Engager (ALiCE), wherein the Fc domain of each heavy chain of immunoglobulin G (IgG) is replaced by the VH and VL domains of an IgG specific to a second antigen while retaining the N-terminal Fab of the parent antibody. Because of specific interactions between the substituted VH and VL domains, the C-terminal stem Fv enables ALiCE to assemble autonomously into hetero-tetramers, thus simultaneously binding to two distinct antigens but with different avidities. This design strategy was used to generate ACE-05 (two anti-PD-L1 Fab × anti-CD3 Fv) and ACE-31 (two anti-CD3 Fab × anti-PD-L1 Fv), both of which bound PD-L1 and CD3. However, ACE-05 was more effective than ACE-31 in reducing off-target toxicity caused by the indiscriminate activation of T cells. Moreover, in cell-based assays and PBMC-reconstituted humanized mice harboring human non-small-cell lung cancer tumors, ACE-05 showed marked antitumor efficacy, causing complete tumor regression at a dose of 0.05 mg/kg body weight. The dual roles of ACE-05 in immune checkpoint inhibition and T-cell redirection, coupled with reduced off-target toxicity, suggest that ACE-05 may be a promising anti-cancer therapeutic agent. Moreover, the bispecific ALiCE platform can be further used for tumor-targeted or multiple immunomodulation applications.

1. Introduction

Antibody-based treatment has become one of the most successful therapeutic strategies for hematologic malignancies and solid tumors. Recently, monoclonal antibodies that target immune checkpoint proteins such as CTLA-4, PD-1, and PD-L1 have shown promising therapeutic outcomes and have become central to cancer immunotherapy [1,2]. Tumorigenesis, however, involves multiple pathological factors and pathways, and antibody-based treatment against a monospecific target (a cellular receptor or a ligand) often leads to acquired resistance to therapy associated with activation or upregulation of compensatory factors and pathways [1,3]. Therefore, dual targeting using bispecific antibodies has emerged as an alternative strategy for cancer therapy. In this context, the clinical success of blinatumomab, a Bispecific T-cell Engager (BiTE) comprising anti-CD19 × anti-CD3, has led to increased interest in the development of bispecific antibodies that redirect the effector functions of various immune cells [2,4]. The challenge of bispecific antibodies has been maintaining desired physicochemical and pharmacokinetic properties while achieving low toxicity as well as high levels of product homogeneity and yield.

In most cases, therapeutic antibodies are immunoglobulins (IgGs) composed of two heavy chains (HCs) and two light chains (LCs). Proper

* Corresponding author. Graduate School of Medical Science & Engineering, KAIST, 291 Daehakro, Yuseong-gu, Daejeon, 34141, South Korea.
** Corresponding author. Y-BIOLOGICS, Inc., 29 Techno 4-ro, Yuseong-gu, Daejeon, 34014, South Korea.
E-mail addresses: parkb2@ybiologics.com (B.-C. Park), hm_kim@kaist.ac.kr (H.M. Kim).

https://doi.org/10.1016/j.biomaterials.2021.120760
Received 3 August 2020; Received in revised form 25 February 2021; Accepted 13 March 2021
Available online 20 March 2021

assembly of these HCs and LCs into a hetero-tetrameric complex is essential for IgG secretion and function. IgG molecules initially assemble as heavy chain dimers, a process mediated by interactions between the two CH3 domains. Therefore, IgGs lacking the CH3 domain do not readily form HC dimers and are often secreted as HC-LC hemimers [5]. Binding of VH with VL is critical for the association of HCs and LCs, as well as for the further folding of CH1 domains on HCs [6]. Notably, VH and VL fragments can also autonomously form stable 1:1 heterodimeric Fv complexes that have the same ability to recognize a specific antigen as the parent antibody [7]. Taking advantage of these characteristics of VH and VL fragments, we here developed a rationally designed, novel, bispecific platform based on IgG, called Antibody-Like Cell Engager (ALiCE). This molecule, with different valency towards two distinct targets, has dual functions—immune checkpoint inhibition and tumor-specific T-cell redirection—thereby exhibiting remarkable anti-tumor efficacy with less off-target toxicity.

2. Materials and methods

2.1. PyMOL analysis of antibody structures

Structures of the anti-CD3 antibody UCHT (PBD ID: 1XIW), the anti-PD-L1 antibody durvalumab (PBD ID: 5 × 8M), and the anti-CTLA-1 antibody ipilimumab (PBD ID: 5TRU) were downloaded from the Protein Data Bank (PBD, www.rcsb.org) and visualized using PyMOL software [8].

2.2. Ethical approval

Animal experiments for pharmacokinetic analyses were conducted using protocols approved by the institutional Animal Care and Use Committee (IACUC) of Qu-BEST BIO, Korea (Approval number, QBSIACUC-A17099). *In vivo* therapeutic efficacy tests in animal models were performed following protocols approved by the Institutional Animal Care and Use Committee (IACUC) of Crown Bioscience (Taicang) Inc., China (Approval number, AN-17020-013-760), and Gempharmatech Co., Ltd., China (Approval number, GPTAP011).

2.3. Construction of ALiCE

The HC pairs, ACE–HC–VH and ACE–HC–VL, of the ALiCE variants ACE-05 (anti-PD-L1 Fab × anti-CD3 Fv), ACE-31 (anti-CD3 Fab × anti-PD-L1 Fv), ACE-18 (anti-CD20 Fab × CD3 Fv) and ACE-00 (anti-HER2 Fab × anti-TNF-α Fv) were generated by PCR-amplifying the sequences encoding VHA-CH1-hinge, VHB and VLB using the parent antibodies YBL-007 (anti-PD-L1), UCHT1 (anti-CD3), rituximab (anti-CD20), Herceptin (anti-HER2), and Humira (anti-TNF-α) as templates. Two PCR fragment pairs, VHA-CH1-hinge and VHB or VHA-CH1-hinge and VLB, were subcloned into the in-house–generated mammalian expression vector p293 F using an Electra cloning system (ATUM) [9] according to the manufacturer's instructions and then were transformed into DH5α competent cells (#CP010, Enzynomics). PCR primers for construction of ALiCE HCs were designed to include a short linker (G4S) between the hinge and VHB or VLB at the 5′ end, and a *Sap*I restriction site, which is necessary for the Electra cloning system, at the 3′ end. The LC used for ALiCE construction, ACE-LC, was identical to the light change of the parent antibody. The sequence encoding the LC containing a leader peptide at the N-terminal was PCR-amplified and subcloned into a p293 expression vector containing a *Nhe*I/*Xho*I restriction site. The resulting constructs were transformed into DH5α competent cells (#CP010, Enzynomics) and confirmed by sequencing.

2.4. Protein expression and purification

For production of the ALiCE variants ACE-00, ACE-05, ACE-18, ACE-31 and BiTE-05 containing a 6x-His tag at the C-terminus, plasmids encoding ACE–HC–VH, ACE–HC–VL and ACE-LC at a ratio of 1:1:2, or BiTE-05, were transfected into FreeStyle 293-F cells (#R79007, ThermoFisher) using polyethylenimine (PEI; #23996–1, Polysciences) at a DNA-to-PEI ratio of 1:4 (w/w) to form polyplexes [10]. For transient transfections, 1 μg of plasmid DNA was transfected into 2 × 10^6 Freestyle 203-F cells, followed by culture in FreeStyle 293 expression medium (#12338018, Gibco) at 37 °C and 5% CO_2 with shaking (120 rpm). ALiCE molecules and BiTE-05 were purified by centrifuging cultures at 4800 rpm for 30 min at 4 °C and subsequently removing debris by filtering supernatants using a 0.22 μm TOP-filter (Millipore). Supernatants containing ALiCE molecules were loaded onto a CaptureSelect CH1-XL pre-packed column (#494346201, ThermoFisher), whereas supernatants containing BiTE-05 were loaded onto Ni-NTA agarose resin (#R90101, ThermoFisher). ALiCE molecules were eluted from the column with 0.1 M glycine (pH 3.0), whereas BiTE-05 was eluted with 3 M imidazole/20 mM sodium phosphate (pH 6.0). Eluted ALiCE molecules and BiTE-05 were dialyzed against phosphate-buffered saline (PBS; pH 7.4) using Slide-A-Lyzer Dialysis Cassette Kits (#66372, ThermoFisher). The Thrombin Cleavage Capture kit (#69022, Merk) was also employed to remove 6x-His-tag from BiTE-05 for SPR binding kinetic assay.

2.5. Analysis of heterodimeric ALiCE

ALiCE molecules were characterized by SDS-PAGE; automated capillary electrophoresis (CE) using an Agilent 2100 Bioanalyzer (Agilent Technology); analytical size-exclusion chromatography (SEC) using a Superdex 200 A column (GE Healthcare Life Science); and analytical cation exchange chromatography (CEX) using a MabPac SCX-10 column (ThermoFisher). Heterodimer formation by two different ALiCE HCs was assessed by analyzing ALiCE molecules with SDS-PAGE and CE under reducing and non-reducing conditions. For CE analysis, a protein-analytic solution mixture was loaded onto a microfluidic protein chip and separated by molecular weight using a Bioanalyzer Protein230 assay kit (Agilent) under reducing and non-reducing conditions, according to the manufacturer's protocol. In addition, the stoichiometric ratios of various chains in ACE-05 were determined under reducing conditions using a Bioanalyzer Protein80 assay kit (Agilent). The average and relative standard deviation (% CV) for the contribution (% total) of each chain to ACE-05, determined from five independent experiments, was analyzed using 2100 Expert Software (Agilent Technology) and plotted using GraphPad Prism 8 software. The quality and conformation of ALiCE molecules were analyzed by SEC (buffer, PBS pH 7.4) using a Superdex 200 A column (GE Healthcare Life Science) and CEX (buffer, 50 mM sodium acetate pH 5.0) using a MabPac SCX-10 column (ThermoFisher). Data were plotted and analyzed using GraphPad Prism 8 software.

2.6. Mass spectrometry

The molecular weight of purified ACE-05 was confirmed by liquid chromatography electrospray ionization with time-of-flight (LC-ESI/TOF) analysis using a ZORBAX 300SB-C8 (2.1 × 50 nm; Agilent) column. The mobile phase consisted of a gradient of water and acetonitrile starting from 5% acetonitrile (initial condition) to 100% acetonitrile over 35 min, with a consistent concentration of 0.2% formic acid over the entire run. The flow rate was 0.1 ml/min. Mass spectrometry detection was performed using a Micro A-TOF III mass spectrometer (Bruker Daltonics, Germany) with electrospray ionization (ESI) in negative mode. The following MS parameters were used: capillary voltage, 4500 V; nebulizer pressure, 0.8 psi; drying gas flow, 5.5/min; and drying gas temperature, 190 °C.

2.7. Protein stability

The thermostability of ACE-05, BiTE-05, YBL-007 and UCHT1 was analyzed using Thermofluor assays [11] with SYPRO orange dye.

Briefly, a 3 μM solution of each purified antibody was mixed with 10 μl of 1:25-diluted SYPRO orange dye (#S6650, ThermoFisher), and 50 μl of each mixture was incubated for 30 min at 25 °C. The samples were denatured by heating at a rate of 1 °C/min from room temperature to 99 °C using a C100 Thermal Cycler, and the amount of CYPRO dye-stained denatured protein was recorded every minute (i.e., each 1 °C temperature change). The melting temperature (TM) was calculated using a CFX 96 ORM system (BioRad). Protein stability was evaluated by exposing CEX-purified ACE-05 to various pH conditions (pH 6, 20 mM sodium phosphate; pH 7.4, PBS; pH 8, 20 mM Tris-HCl) or long incubation (7 days) at room temperature and then analyzing by CEX-HPLC using a MabPac SCX-10 analytic column (ThermoFisher). Data were plotted using GraphPad Prism 8 software.

2.8. Determination of binding kinetics

The binding kinetics of ALiCE molecules to various antigens were measured by surface plasmon resonance using a Biacore 8 K system equipped with certified-grade CM5 series S sensor chips (#BR100399, GE Healthcare) [12–15]. HEPES-buffered saline (0.01 M HEPES, 0.15 M NaCl) containing 3 mM ethylenediaminetetraacetic acid (EDTA) and 0.05% (v/v) P20 detergent (HBS-EP+) was used as reaction and running buffer (#BR100669, GE Healthcare). The antigens PD-L1-his (0.1 μg/ml; synthesized in-house) and CD3εδ-flag-his (0.2 μg/ml; #CT038-H2508H, Sino Biological) were immobilized on the surface of a CM5 sensor chip (#BR100399, GE Healthcare) according to the manufacturer's instruction. Thereafter, bispecific T-cell engagers (ACE-05, BiTE-05, and ACE-31) and parent mAb (YBL-007 and UCHT1), diluted in HBS-EP + buffer, were applied over antigen-immobilized sensor chips at 12 different concentrations (0, 0.5, 1, 2, 4, 8, 16, 32, 64, 128, 256, and 512 nM) for 300 s at a flow rate of 30 μl/min. Analytes bound to sensor chips were dissociated by washing with HBS-EP + running buffer for 300 s. Associations ($M^{-1}s^{-1}$, K_a) and dissociations (S^{-1}, K_d) were both measured over 300-s intervals. The equilibrium dissociation constant (M, K_D) was calculated as the ratio of off-rate to on-rate (k_d/k_a). Kinetic parameters were determined with the global fitting function of Biacore Insight Evaluation Software using a 1:1 binding model for monovalent ligand-analyte interactions and a 1:2 binding model for bivalent ligand-analyte interactions.

2.9. Simultaneous binding analysis

For simultaneous dual binding analysis of ACE-05 and ACE-31 toward CD3 and PD-L1, biolayer light interferometry was performed on an Octet QKe system (Pall Forte Bio) [14,15]. The first ligands, PD-L1-Fc (2 μg/ml; synthesized in-house) and CD3εδ-flag-his (3 μg/ml; #CT038-H2508H, Sino Biological), were loaded onto hydrated AHC (#18–5064, Pall Forte Bio) or Ni-NTA (#18–5013, Pall Forte Bio) biosensors, respectively, until binding reached 0.5–1.0 nM. The biosensors were then washed with kinetics buffer (PBS containing 0.1% bovine serum albumen [BSA] and 0.02% Tween-20) for 2 min (ACE-05) or 1 min (ACE-31) to remove any unbound proteins, immersed in 30 nM ACE-05 or 15 nM ACE-31 to analyze associations, and washed with PBS for 7 min (ACE-05) or 2 min (ACE-31) to measure dissociation. Biosensors loaded with the first ligand and ACE-05 or ACE-31 were subsequently immersed in solution containing the second ligand, either 200 nM CD3εδ-flag-his (ACE-05) or 120 nM PD-L1-Fc (ACE-31), to measure association, followed by washing with PBS for 3 min (ACE-05) or 2 min (ACE-31) to measure dissociation. Sensorgram data were plotted using GraphPad Prism software 8.

2.10. Flow cytometry

To evaluate the level of cell surface PD-L1, we incubated PD-L1$^+$ cancer cells (HCC827, MDA-MB-231, and Karpas-299) and PD-L1$^-$ Raji cells, all at 0.5×10^6 cells/100 μl, with 1:50 (v/v)-diluted phycoerythrin (PE)-Cy7–conjugated anti-PD-L1 antibody (#55817, BD Bioscience). A fluorescein isothiocyanate (FITC)-conjugated anti-CD3 antibody (#130-113-138, Miltenyi Biotech) was used for assessment of CD3 levels on Jurkat T cells (0.5×10^6 cells/100 μl). The cells were washed twice with 1 ml FACS buffer (PBS containing 1% fetal bovine serum [FBS]) and cell surface expression of PD-L1 or CD3 was analyzed by flow cytometry (BD FACSCanto II). The dual binding ability of ACE-05 and ACE-31 for PD-L1 and CD3 on the cell surface was investigated by incubating 20 nM ACE-05, ACE-31 or ACE-18 (CD20 Fab × CD3 Fv, Ctrl-ACE) with CD3$^+$ Jurkat T cells for 1 h. After two washes with 1 ml FACS buffer, cells were incubated with PD-L1-Fc (75 μg/100 μl) and washed twice with 1 ml FACS buffer. PD-L1-Fc was then detected using Alexa 647-conjugated anti-human Fc antibody (#109-605-098, Jackson ImmunoResearch). The apparent binding affinity of ALiCEs (ACE-05 and ACE-31) for PD-L1$^+$ Karpas-299 and PD-L1$^-$ Raji cancer cells and CD3$^+$ Jurkat T cells was measured by treating these cells (0.5×10^6 cells/100 μl) with the indicated concentrations of ACE-05 (0.000932, 0.003729, 0.014915, 0.059662, 0.59459, 3.81, and 15.27 nM for Karpas-299; 1.56, 15.625, 156.25, and 1562 nM for Raji; 1.1, 3.3, 9.9, 29.6, 88.9, 266.7, 800, and 2400 nM for Jurkat) or ACE-31 (0.594, 3.81, 15.27, 61.03, 244.37, 977.5, and 3910 nM for Karpas-299; 1.56, 15.625, 156.25, and 1562 nM for Raji; 0.011, 0.033, 0.101, 0.304, 0.914, 2.743, 8.320, 24.691, and 74.074 nM for Jurkat). Cell surface-bound ACE-05 or ACE-31 was detected by flow cytometry (CytoPLEX-LX) following incubation with Alexa 647-conjugated antibody against human Fab fragment (#109-606-097, Jackson Immunoresearch). Flow cytometry data were analyzed using FlowJo 10 software (FlowJo, LLC), and geometric means were plotted using GraphPad Prism 8 software.

2.11. Jurkat T cell activation by ALiCE (ACE-05 and ACE-31)

To assess whether ACE-05 and ACE-31 redirected T-cell activation against PD-L1 on target cell surfaces, we seeded PD-L1$^-$ WT HEK cells or genetically engineered PD-L1$^+$ HEK cells (7×10^4 cells/well) onto white-bottomed plates coated with poly-L-lysine (#P4707, Sigma). After pre-incubating these cells for 24 h, PD-1$^-$ Jurkat T cells (2×10^5 cells/well) expressing the firefly luciferase gene under control of an NFAT-response element and serial dilutions of ACE-05, ACE-31, or BiTE-05 were added and cells were incubated for 6 h at 37 °C and 5% CO_2. Luciferase accumulation induced by T cell activation was then measured by performing Bio-Glo Luciferase assays (#G7940, Promega) according to the manufacturer's protocol [16]. The resulting data, expressed in relative light units (RLU), were plotted and analyzed using GraphPad Prism 8 software.

2.12. On-target T cell activation

To assess on-target specific T cell activation, we co-cultured PD-L1$^+$ MDA-BM-231 cancer cells (1×10^5 cells/well) and CD3$^+$ T cells (1×10^6 cells/well) isolated from human PBMCs (#SER-PBMC-200-F, Zenbio) in medium containing 5% FBS, to which 1 nM ACE-05, BiTE-05, ACE-31 or IgG was added. CD3$^+$ T cells were stained with Trace Far Red (#C34564, ThermoFisher) according to the manufacturer's instructions. After incubating for 24 or 48 h, T cells were harvested and labeled with APC-conjugated anti-CD4 antibody (#130-113-210, MiltenyBiotec), FITC-conjugated anti-CD8 antibody (#130-110-677, MiltenyBiotec), PE-Vio 770-conjugated anti-CD69 (#130-122-5-4, MiltenyBiotec) antibody and PE-conjugated anti-CD25 antibody (#341009, BD Bioscience). T cell subsets and activated T cells were identified by flow cytometry (BD FACSCanto II) with the aid of FlowJo 10 software (FlowJo, LLC).

2.13. PD-1/PD-L1 blockade bioassay

PD-1/PD-L1 blockade bioassays was performed according to the manufacturer's protocol (#J1250, Promega) [17]. Briefly, one vial of PD-L1/aAPC$^+$ CHO–K1 cells in the bioassay kit were suspended in

recovery medium (90% Ham's F-12 containing 10% FBS) from frozen stocks, seeded onto white-bottomed plates, and incubated overnight at 37 °C. To each well was added Jurkat T cells stably expressing human PD-1 and NFAT-luciferase reporter in assay buffer (RPMI 1640 containing 1% FBS), together with ACE-05, BiTE-05, ACE-31, YBL-007 or IgG at concentrations of 0, 0.006, 0.032, 0.16, 0.8, 4 or 20 nM. After 6 h, NFAT-mediated luciferase activity was measured using a Bio-Glo luciferase assay system (#G7940, Promega). RLU data were plotted and analyzed using GraphPad Prism 8 software.

2.14. Tumor-killing assay

HCC827 (ATCC CRL2868), MDA-MB-231 (ATCC HTB-26), Karpas-299 (#06072604, Sigma) and Raji (ATCC CCL86) cancer cells were maintained in RPMI-1640 medium supplemented with 10% FBS at 37 °C, 5% CO_2. All healthy donor PBMCs and $CD8^+$ T cells used in this study were purchased from AllCells (#PB004F and #PB009–3 F), Zenbio (#SER-PBMC-200-F), and Lonza (#3W-270). $CD3^+$ T cells and $CD8^+$ T cells were isolated from human PBMC preparations using a Pan T-cell isolation kit (#130-096-535, Miltenyi Biotec) and a $CD8^+$ T-cell isolation kit (#130-096-495, Miltenyi Biotec). PBMC or T-cell cytotoxicity against PD-L1–expressing cancer cells was assessed by measuring lactate dehydrogenase (LDH) released from dead cancer cells [18]. The on-target tumor cell-killing ability of bispecific T-cell engagers was investigated by co-incubating PD-$L1^+$ MDA-MB-231 cancer cells (1×10^4 cells/well) and T cells at an E:T (effector:target) ratio of 10:1 ($CD3^+$ T cells) or 5:1 ($CD8^+$ T cells) with the indicated proteins (ACE-05, ACE-31, BiTE-05, or IgG). After incubating for 48–72 h, LDH released from dead tumor cells was measured using CytoTox96 non-radioactive cytotoxicity assay kits (#G1780, Promega) according to the manufacturer's instructions. The percentage of dead tumor cells was calculated using the formula, % Cytotoxicity (% dead tumor cells) = (experimental – target spontaneous – effector spontaneous)/(target maximum – target spontaneous) × 100%. PBMCs were also used as effector cells (E:T ratio, 25:1) to investigate PD-$L1^+$ HCC827 tumor cell-killing ability. For evaluation of off-target T-cell cytotoxicity, PD-$L1^-$ HEK293 or Raji cancer cells were co-cultured with $CD3^+$ T cells and 1 nM ACE-05, BiTE-05, ACE-31, IgG, or ACE-18. After incubating for 48–72 h, LDH released from PD-$L1^-$ cells were measured and calculated as described above.

2.15. T-cell clustering

T-cell activation and differentiation was evaluated by accurately quantifying T cell and PD-$L1^+$ tumor cell clustering using an IncuCyte live-cell analysis system (Sartorius, USA). $CD3^+$ T cells were isolated from human PBMCs and labeled with CytoLight reagent (#4706, Sartorius) according to the manufacturer's protocol. PD-$L1^+$ MDA-MB-231 cells (4×10^3 cells/well) and $CD3^+$ T cells were co-cultured at an E:T ratio of 10:1 together with 1 nM ACE-05, ACE-31, BiTE-05, or IgG. Live-cell images were obtained every 6 h during the 90-h incubation period, and the average area of red fluorescent clusters (μm^2) indicative of T-cell activation was measured using IncuCyte software. Data obtained from quadruplicates were plotted using GraphPad Prism 8 software.

2.16. T-cell expansion

ACE-05–induced primary human T-cell expansion in the presence of PD-$L1^+$ tumor cells were investigated using T-cell proliferation assays. $CD3^+$ T cells isolated from PBMCs were stained with Cell Trace Far Red (#C34564, ThermoFisher) according to the manufacturer's instructions. PD-$L1^+$ MDA-MB-231 cancer cells were seeded in 24-well plate at a density of 1×10^5 cells/well. The next day, pre-incubated MDA-MB-231 cells were washed once with pre-warmed Dulbecco's PBS, which was then replaced with assay medium (RPMI-1640 containing 1% FBS). Cell Trace-stained $CD3^+$ T cells (1×10^6 cells/well) and a mixture containing 1 nM ACE-05, IgG or ACE-18 (CD20 × CD3, as a negative control) was then added to MDA-MB-231 cells in 24-well plates. After incubating for 96 h, T cells were harvested and analyzed by flow cytometry using a BD FACSCanto II system. The expansion of T cells was visualized based on the obtained flow cytometry data using FlowJo 10 software (FlowJo, LLC).

2.17. Off-target T-cell activation by multimeric T-cell engagers in the absence of tumor cells

To evaluate non-specific off-target T-cell activation by T-cell engagers in the absence of target tumor cells, we cultured $CD3^+$ T cells (1×10^6 cells/well) isolated from human PBMCs (#4 W–270C, Lonza) in medium containing 5% FBS, to which 1 nM ACE-05, BiTE-05 or multimeric ACE-05 was directly added. Clustered ACE-05 was prepared by mixing 5 μl CH1 beads (#1943462250, ThermoFisher) with 1 nM ACE-05. After incubating for 48 h, T cells were harvested and labeled with a FITC-conjugated CD4 antibody (#130-114-531, MiltenyBiotec) and CD69-PE-Vio 770 (#130-122-5-4, MiltenyBiotec) antibody. T cell subsets and activated T cells were identified by flow cytometry (BD FACSCanto II) with the aid of FlowJo 10 software (FlowJo, LLC).

2.18. Immune cell-released cytokines

Levels of the cytokines, IL-2, IFN-γ, IL-6 and TNF-α, released from activated immune cells (PBMCs and $CD4^+$ T cells) were investigated in the presence or absence of PD-$L1^+$ tumor cells. In the presence of PD-$L1^+$ HCC827 cancer cells—the on-target condition—human PBMCs were co-cultured for 72 h with HCC827 cancer cells at an E:T ratio of 25:1 together with 1 nM ACE-05, BiTE-05, ACE-31, or IgG. Samples were collected at specific time points (0, 6, 12, 18, 24, 48, and 72 h), and the concentrations of cytokines were determined using ELISA kits for IL-2 (#431004, BioLegend), IFN-γ (#430104, BioLegend), IL-6 (#430504, BioLegend) and TNF-α (#430204, BioLegend), according to the manufacturer's protocols. For the off-target condition, 1 nM ACE-05, BiTE-05, ACE-31, or IgG was directly added to $CD4^+$ T cells, isolated from human PBMCs using a $CD4^+$ T cell isolation kit (#130-096-533, Miltenyi Biotec). After incubating for 72 h, the released cytokines were measured by ELISA as described above. For measurement of granzyme B, PBMC-derived $CD8^+$ T cells and MDA-MB-231 cells were co-cultured at an E:T ratio of 5:1 together with different amounts (0, 6.4, 32, 160, 800, and 4000 pM) of ACE-05, BiTE-05, ACE-31, or IgG. After 48 h, granzyme B accumulated in the assay medium was measured using an ELISA kit (#DGZB00, R&D Systems). The optical density (OD) of each supernatant was measured using a microplate reader, and the concentrations of cytokines were analyzed using GraphPad Prism 8 software.

2.19. Pharmacokinetics in rats and cynomolgus monkeys

Male Sprague-Dawley rats, aged 6–7 weeks, were injected with a single 10-mg/kg dose of ACE-05, BiTE-05 or hIgG via the tail vein (n = 3/group). Blood samples (150 μl each) were collected from each animal at 10 and 30 min; 1, 2, 4, 8, and 24 h; and 3, 5, and 9 days, and centrifuged at 10,000–13,000 rpm for 2 min. A 70-μl aliquot of each plasma sample was stored at −80 °C until further analysis. Male cynomolgus monkey, aged 20–24 months, were intravenously administered a single 5-mg/kg dose of ACE-05, BiTE-05 or hIgG (n = 3/group). Blood samples were collected from each animal at the indicated time points (10 and 30 min; 1, 2, 4, 8 and 24 h; and 2, 3, 4, 8, 12 and 15 days). Pharmacokinetic analyses were performed using a Gyrolab xPlore automated immunoassay system [19]. Biotinylated anti-human IgG CH1 nanobody for capture of ACE-05 or human IgG was immobilized on the surface of streptavidin-coated Gyrolab Bioaffy CD200 (#P0004180, Gyros Protein Technologies), and serum samples were loaded. Similarly, biotinylated PD-L1-Fc was used to capture BiTE-05. Captured ACE-05

and human IgG were detected using Alexa 647-conjugated anti-kappa antibody (#316514, Novus), and BiTE-05 was detected using Alexa 647-conjugated anti-His antibody (#362611, Novus). Concentrations of samples were calculated using Gyrolab software, and $t_{1/2}$ values were calculated using Phoenix WinNonlin software.

2.20. Anti-tumor efficacy of ALiCE in a humanized mouse model

The anti-tumor efficacy of ALiCE against PD-L1$^+$ HCC827 tumors was assessed in a PBMC-reconstituted humanized NCG mouse model. Briefly, female NCG mice (Crown Bioscience) aged 7–8 weeks were randomly divided into four groups of 10 mice each. Each mouse was intravenously engrafted with 5×10^6 cells/100 μl PBMCs isolated from two healthy donors. Three days later, mice were inoculated subcutaneously in their right flank region with 5×10^6 PD-L1$^+$ HCC827 tumor cells. When tumor volumes reached ~50 mm^3 (4 days later), mice were injected with ACE-05 or BiTE-05 every other day (Q2d, 3 doses total) or with YBL-007 or IgG every third day (Q3d, 3 doses total). Tumor dimensions and body weights were measured every 2 days and plotted against time using GraphPad Prism 8 software.

2.21. Cytokine analysis in vivo

Female non-tumor–bearing hCD3ε TG mice, aged 6–7 weeks, were divided into 4 groups of 6 mice each and injected with a single 0.5-mg/kg dose of ACE-05 or BiTE-05 or 5 mg/kg dose of IgG via the tail vein. Blood samples for cytokine analysis were collected from each animal at specific time points (0, 6, 12, 24, and 48 h) and stored at −80 °C until further analysis. Multiple cytokines in each collected plasma samples were analyzed using a BD Cytometric Bead Array (CBA) Mouse Inflammation Kit (#552364, BD Bioscience) and Mouse Th1/Th2 Cytokine Kit (#551287, BD Bioscience) according to the manufacturer's protocol. The calculated levels of cytokines were plotted using GraphPad Prism 8 software.

2.22. Tumor-infiltrating lymphocytes (TILs)

Tumor-infiltrating lymphocytes were analyzed in hCD3ε TG mice bearing hPD-L1–expressing CT26 tumors. Mice were inoculated subcutaneously in their right flank region with 5×10^5 CT26-hPD-L1 cells. When the subcutaneous tumor volume reached ~90 mm^3, intraperitoneal (i.p.) administration of test formulations (ACE-05, 1 mg/kg; YBL-007, 3 mg/kg; UCHT1, 2 mg/kg) was started and continued twice a week for 2 weeks (BIW, 4 doses total). One week after the last injection, tumors were collected from mice and manually dissected. The percentage/number of live lymphocytes and T cell subsets in tumor tissues were analyzed by flow cytometry using multiple lymphocytes markers (mCD45, mCD4, mCD8, and hCD3), and the results were plotted using GraphPad Prism 8 software.

2.23. In silico immunogenicity prediction

Class I immunogenicity of ACE-05-HC-VH and ACE-05-HC-VL chains was investigated using the *in silico* web-based prediction tools, MHC-I Binding Predictions (http://tools.iedb.org/mhci/) and Class I Immunogenicity (http://tools.iedb.org/immunogenicity/). For MHC-I binding, epitope candidates were predicted from an analysis of the amino acid sequences of ACE-05-HC-VH and ACE-05-HC-VL based on peptide processing in the cell using the IEDB (Immune Epitope Database) recommended prediction method [20]. Only 8–10mer peptides with 0.3 percentile rank cut-off were selected as possible peptides presented on MHC class-I molecules. Immunogenicity scores of selected peptide sequences were then obtained using the MHC-I Binding Predictions tool [21]. Possible immunogenic peptides (score > 0) as well as their positions within ACE-05-HC-VH and ACE-05-HC-VL chains were identified.

2.24. Statistics

Data from cell line experiments are presented as means ± standard error of the mean (SEM) and were compared using ordinary one-way ANOVA with Dunnett's multiple compassion test or Mann-Whitney tests. Statistical values in graphs indicating means and errors were plotted using GraphPad Prism 8 software.

3. Results

3.1. Generation of ALiCE molecules based on VH-VL heterodimer formation

Crystal structures of various VH and VL complexes, including the anti-CD3 antibody UCHT1 (PDB ID: 1XIW), anti-PD-L1 antibody durvalumab (PDB ID: 5X8M) and anti-CTLA4 antibody ipilimumab (PDB ID: 5TRU), clearly demonstrate that the key determinant of VH and VL interaction is the CDR3 region of VH, which binds to CDR1, -2 and -3 regions of VL by forming a "Knob-into-Hole" structure (Fig. 1A) [22–25]. Moreover, hydrophobic interactions surrounded by electrostatic interactions at the VH-VL interface contribute to the autonomous assembly of VH and VL domains and the stabilization of Fv complexes (Fig. S1).

Despite the significant role of CH3 domains in antibody assembly, we hypothesized that this autonomous assembly of VH and VL domains as well as stable Fv complex formation not only facilitates the specific hetero-dimerization of two HCs, but can also be utilized to introduce additional sites for binding a second antigen. To test this, we replaced the Fc domains of the two HCs of the parent IgG with the VH and VL domain of an IgG specific to a second antigen, creating ACE–HC–VH and ACE–HC–VL, respectively (Fig. 1B). As test systems, we used the anti-CD3 antibody UCHT1 and an in-house–screened anti-PD-L1 antibody, termed YBL-007, whose PD-L1/PD-1 signal-blocking ability is similar to that of avelumab (Fig. S2A). In addition, YBL-007 can recognize both human and murine PD-L1 with similar binding affinity (Fig. S2B). The LC of the parent YBL-007 was used for ACE-LC, and VH-CH1 as well as hinge regions of YBL-007 HC were fused to VH or VL of UCHT1 to generate the two HCs of ALiCE. Various combinations of expression vectors encoding ACE–HC–VH, ACE–HC–VL and ACE-LC were transfected into FreeStyle 293-F cells, and expression of these molecules in culture medium was analyzed by SDS-PAGE and Western blotting (Fig. 1C). As expected, none of the individual chains could be expressed, likely owing to both folding and secretion problems (Fig. 1C, lanes 1–3). Moreover, ACE–HC–VH chains with a knob structure on the CDR3 loop of the UCHT1 VH domain could not assemble into homodimers owing to incongruent knob-knob interactions (Fig. 1C, lane 4), whereas homodimer formation between identical ACE–HC–VL chains was barely detectable (Fig. 1C, lane 5). Interestingly, a properly assembled complex was highly expressed and secreted only in the presence of ACE–HC–VL, ACE–HC–VH, and ACE-LC together (Fig. 1C, lane 6). The resulting ALiCE (anti-PD-L1 Fab × anti-CD3 Fv), hereinafter termed ACE-05, was transiently expressed in FreeStyle 293-F cells and purified by CH1 affinity chromatography, with a yield of ~20–30 mg/L. Capillary electrophoresis analyses using a Bioanalyzer assay kit (P230 and P80 kit) under reducing and non-reducing conditions showed that ACE-LC, ACE–HC–VH and ACE–HC–VL chains were present at a 2:1:1 ratio in ACE-05 (Fig. 1D and E). Size-exclusion chromatography and mass spectrometry (MS) analysis with LC-ESI/TOF showed that ACE-05 was a uniform heterotetramer (Fig. 1D and F). Specifically, the observed mass of the main peak (123,997 Da) was very close to the theoretical mass of the heterotetrameric structure of ACE-05 (123,942 Da); by comparison, the mass of the homotetrameric structure, ACE-05-HC-VH homodimer + two ACE-05-LCs was 125,597 Da and that of ACE-05-HC-VL homodimer + two ACE-05-LCs was 122,287 Da (Fig. 1F). These results confirm the absence of detectable homotetrameric complexes in purified ACE-05.

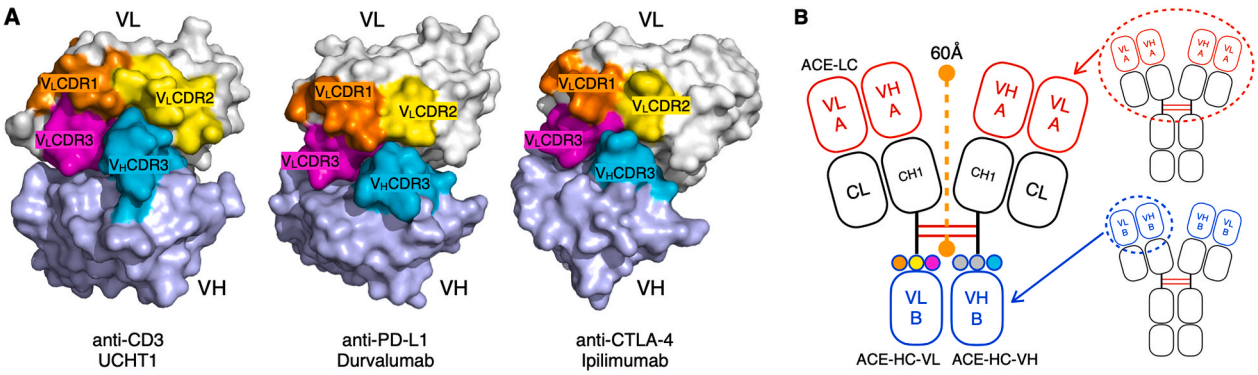

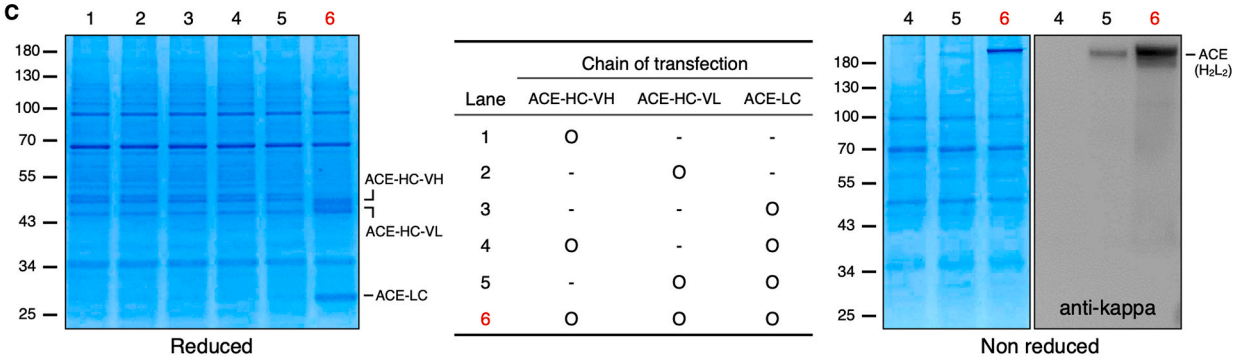

Lane	Chain of transfection: ACE-HC-VH	ACE-HC-VL	ACE-LC
1	O	-	-
2	-	O	-
3	-	-	O
4	O	-	O
5	-	O	O
6	O	O	O

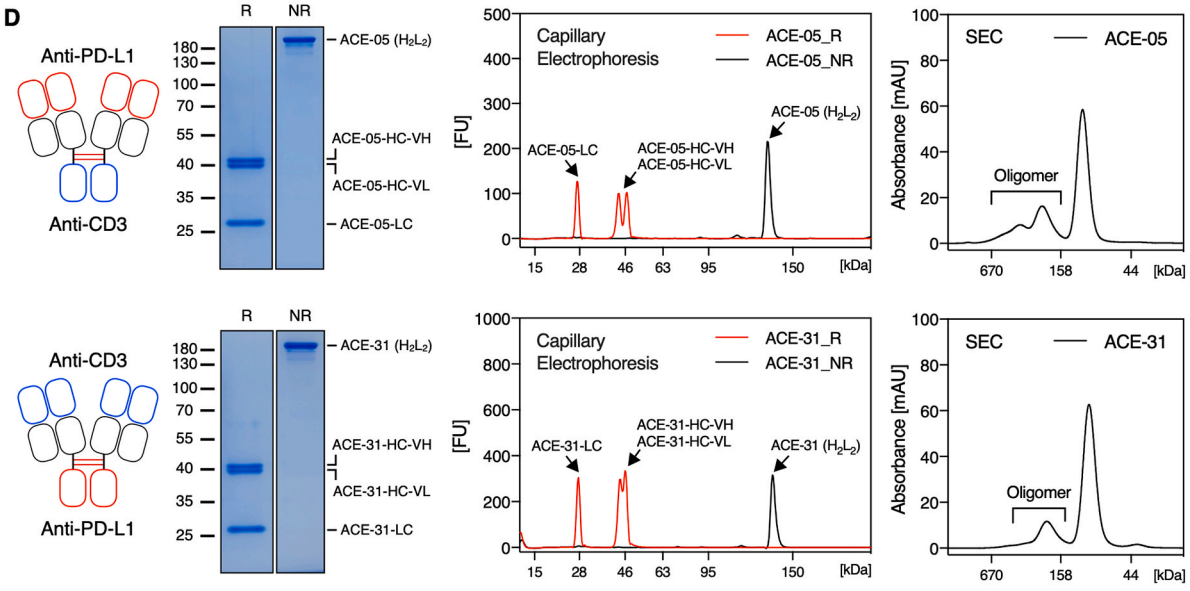

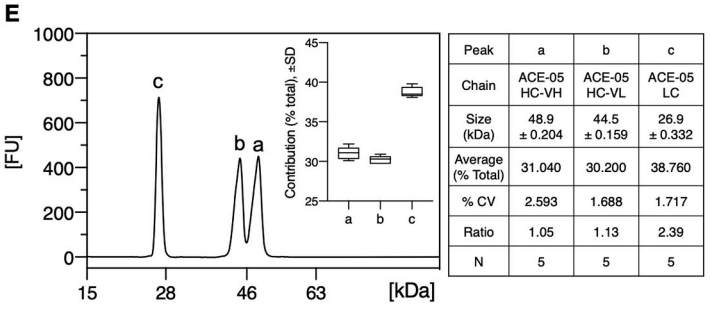

Peak	a	b	c
Chain	ACE-05 HC-VH	ACE-05 HC-VL	ACE-05 LC
Size (kDa)	48.9 ± 0.204	44.5 ± 0.159	26.9 ± 0.332
Average (% Total)	31.040	30.200	38.760
% CV	2.593	1.688	1.717
Ratio	1.05	1.13	2.39
N	5	5	5

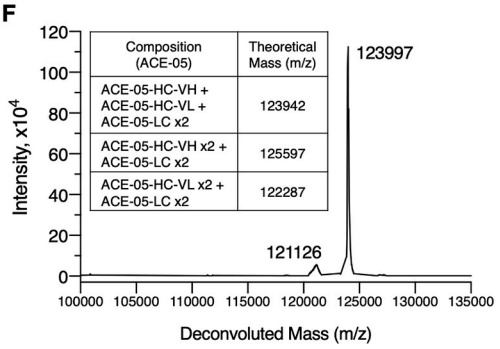

Composition (ACE-05)	Theoretical Mass (m/z)
ACE-05-HC-VH + ACE-05-HC-VL + ACE-05-LC x2	123942
ACE-05-HC-VH x2 + ACE-05-LC x2	125597
ACE-05-HC-VL x2 + ACE-05-LC x2	122287

(caption on next page)

Fig. 1. Design and production of the bispecific T-cell engager, ALiCE. (A) "Knob-into-Hole" structure of the variable domain of the anti-CD3 antibody UCHT1 (PBD ID: 1XIW), anti-PD-L1 antibody durvalumab (PBD ID: 5X8M), and anti-CTLA-4 antibody ipilimumab (PBD ID: 5TRU). CDR loops are color-coded as follows: VH CDR3, cyan; VL CDR1, orange; VL CDR2, yellow; and VL CDR3, magenta. (B) Schematic diagram of ALiCE, which is composed of two identical LCs (ACE-LC) and two different HCs (ACE–HC–VL and ACE–HC–VH). (C) Expression of ACE–HC–VH, ACE–HC–VL and ACE-LC chains in FreeStyle 293-F cells. Proteins in cell supernatants were resolved by SDS-PAGE under reducing (left) and non-reducing (right) conditions. Properly assembled ALiCE was detected by Western blotting using an HRP-conjugated anti-kappa antibody. (D) ACE-05 (anti-PD-L1 Fab × anti-CD3 Fv) and ACE-31 (anti-CD3 Fab × anti-PD-L1 Fv), purified by CH1 affinity chromatography, were analyzed by SDS-PAGE (left) and capillary electrophoresis (middle) under reducing and non-reducing conditions. Size-exclusion chromatography of non-reduced ACE-05 and ACE-31 (right). (E) Capillary electrophoresis using a Bioanalyzer 2100 system. The stoichiometric ratio of the three chains in ACE-05 (ACE-05-HC-VH, ACE-05-HC-VL, ACE-05-LC) under reducing conditions was measured by automated capillary electrophoresis (CE) using a Bioanalyzer Protein80 assay kit. Representative CE results are presented (left). Average and relative standard deviation (%CV) for the contribution (% total) of each chain to ACE-05 from five independent experiments are presented in the inset and table (right). (F) Mass spectrometry analysis of the hetero-tetrameric structure of ACE-05. After CH1 affinity chromatography followed by cation exchange chromatography (CEX) purification, ACE-05 was analyzed by LC-MS and ESI-TOF. The deconvoluted spectrum of the mass range 100,000–135,000 *m/z* is shown, and the theoretical masses of possible combinations (ACE-05-HC-VH + ACE-05-HC-VL + two ACE-05-LC; ACE-05-HC-VH homodimer + two ACE-05-LC; ACE-05-HC-VL homodimer + two ACE-05-LC) are indicated in the inset table.

We also investigated whether the ALiCE platform can be generally applied to other antibody pairs by generating ACE-31 (anti-CD3 Fab × anti-PD-L1 Fv with UCHT1 and YBL-007) and ACE-00 (anti-HER2 Fab × anti-TNF-α Fv with anti-HER2 mAb [Herceptin] and anti-TNF-α mAb [Humira]). Similar to ACE-05, ACE-31 and ACE-00 assembled as the corresponding hetero-tetrameric complexes, ACE–HC–VL, ACE–HC–VH and two ACE-LCs, and were secreted as homogeneous forms (Fig. 1D and Fig. S2D).

During protein expression, a small amount of aggregation (or misfolding of oligomers) occurred (Fig. S2E). However, these aggregates were easily removed by cation exchange chromatography (CEX) and further aggregation does not occur after CEX purification. Stability tests of ACE-05 using thermostability analyses and exposure to various pH conditions (pH6–8) or long incubation (7 days) at room temperature showed that ACE-05 is a stable and homogeneous structure, similar to IgG (Fig. S3A and S3B).

3.2. Binding kinetics and concurrent binding ability of ALiCE as a T-cell engager

The distance between the outer and inner binding domains of ALiCE was found to be approximately 60 Å, a distance that would likely allow formation of an immunologic synaptic bridge between the tumor and effector cells [23,26–29] (Fig. 1B and Fig. S4). Given that the preferential binding of bispecific T-cell engager to a tumor cells over T-cells, which can mediate the reduced off-target T-cell cytotoxicity, is a function of the relative binding affinity, we analyzed the binding kinetics of ACE-05 (anti-PD-L1 Fab × anti-CD3 Fv) and ACE-31 (anti-CD3 Fab × anti-PD-L1 Fv) to PD-L1 and CD3 by surface plasmon resonance using a Biacore 8 K system (GE Healthcare) and compared them with the binding kinetics of YBL-007 (anti-PD-L1 parent antibody), UCHT1 (anti-CD3 parent antibody) and BiTE-05 (anti-PD-L1 × anti-CD3) to the same antigens (Fig. 2A and Fig. S5A). We found that the binding affinity (K_D) of ACE-05 for PD-L1 (6.78×10^{-10} M) was comparable to that of YBL-007 (6.46×10^{-10} M), but higher than that of BiTE-05 (1.39×10^{-9} M), probably owing to the two PD-L1 binding sites on ACE-05 and YBL-007. Moreover, the comparison of binding affinity of ACE-05, YBL-007, and monovalent YBL-007 Fab to PD-L1 confirmed that the higher valency (avidity) can lead to the increased binding affinity (Fig. S5B). Similarly, the binding affinities of CD3 for ACE-31 (2.39×10^{-10} M) and UCHT1 (2.65×10^{-10} M), both of which contain bivalent anti-CD3 Fab arms, were higher than that for BiTE-05 (1.01×10^{-9} M). In contrast, the binding affinities of the monovalent stem Fv of ACE-05 for CD3 (2.15×10^{-8} M) and of ACE-31 for PD-L1 (2.72×10^{-8} M) were 40–80 fold lower than those of the parent antibodies UCHT1 and YBL-007 for CD3 (2.65×10^{-10} M) and PD-L1 (6.46×10^{-10} M), respectively. More interestingly, the binding affinity of stem Fv of ACE-05 for CD3 and ACE-31 for PD-L1 were even lower than that of BiTE-05 for CD3 (1.01×10^{-9} M) and PD-L1 (1.39×10^{-9} M), likely owing to steric hindrance between the Fab arms and the second antigen-binding region of stem Fv. However, using biolayer light interferometry on an Octet QKe system (Pall Forte Bio) and flow cytometry (GE Healthcare), we confirmed the concurrent binding of ACE-05 and ACE-31 to both PD-L1 and CD3 (Fig. 2B and Fig. S5C), indicating that the binding affinities for the two respective antigens were dependent on the valency of ALiCE paratopes.

Next, we investigated the effects of the valency of ALiCE paratopes on tumor and T-cell binding. The apparent binding affinities of ACE-05 or ACE-31 for PD-L1 on Karpas-299 tumor cells and CD3 on Jurkat T cells were consistent with their *in vitro* binding affinities for PD-L1 and CD3, with ACE-05 exhibiting stronger binding to PD-L1 ($K_D = 31.45$ pM to PD-L1$^+$ Karpas-299 cells) and weaker binding to CD3 ($K_D = 52.44$ nM to CD3$^+$ Jurkat T cells) compared with the corresponding binding affinities of ACE-31 ($K_D = 20.58$ nM to PD-L1$^+$ Karpas-299 cells and $K_D =$ 856 pM to CD3$^+$ Jurkat T cells); neither ACE-05 nor ACE-31 bound to PD-L1$^-$ Raji cells (Fig. 2C).

3.3. Enhanced tumor cell killing and reduced non-specific T-cell toxicity of ACE-05

To compare on-target and off-target T-cell activation by ACE-05, ACE-31 and BiTE-05, we co-cultured wild-type (WT) PD-L1$^-$ HEK cells or genetically engineered PD-L1$^+$ HEK cells with PD-1$^-$ Jurkat T cells expressing an NFAT-luciferase reporter gene (Fig. S6A). We then assessed Jurkat T-cell activation following treatment with the T-cell engagers ACE-05, ACE-31 or BiTE-05 by measuring NFAT-luciferase reporter activity. Interestingly, ACE-05 exhibited the highest on-target NFAT activation when co-cultured with PD-L1$^+$ HEK and PD-1$^-$ Jurkat T cells, whereas BiTE-05 and ACE-31 showed higher off-target T-cell activation than ACE-05 when co-cultured with WT PD-L1$^-$ HEK and PD-1$^-$ Jurkat T cells, effects mediated by direct binding to CD3 on Jurkat T cells in the absence of PD-L1 targeting (Fig. 3A).

According to concurrent binding of ACE-05, ACE-31 and BiTE-05 to both PD-L1 and CD3, but with different affinity, we investigated their ability to inhibit the PD-1/PD-L1 interaction as well as to induce PD-L1/CD3–mediated T-cell redirection/activation using Jurkat T cells stably expressing PD-1 and an NFAT-luciferase reporter and CHO–K1 cells expressing human PD-L1 and an engineered cell surface protein designed to activate cognate T-cell receptors (TCRs) in an antigen-independent manner [30]. As expected, T-cell activation was higher following treatment of these cultures with ACE-05 or BiTE-05 than following treatment with YBL-007, with the latter only able to disrupt PD-L1/PD-1 interactions (Fig. 3B). These results imply the significance of the dual-target specificities of ACE-05 and BiTE-05 that enable inhibition of PD-L1/PD-1 interactions and PD-L1/CD3–mediated T-cell redirection, simultaneously. Of note, the T-cell activation efficiency of ACE-05, containing bivalent anti-PD-L1 Fab arms ($EC_{50} = 0.21$ nM), was 5-times higher than that of BiTE-05, containing a monovalent anti-PD-L1 scFv ($EC_{50} = 1.09$ nM). However, ACE-31 was much less effective than ACE-05, BiTE-05 and YBL-007 in re-activating T cells (Fig. 3B, gold line), demonstrating that tight binding to PD-L1 positive cell for T-cell redirection and inhibition of PD-1/PD-L1 axis is critical for

A

Antibody	Binding affinity to PD-L1					Binding affinity to CD3				
	K_D(M)	K_a($M^{-1}s^{1}$)	K_d(s^{-1})	Chi^2	R_{max}	K_D(M)	K_a($M^{-1}s^{1}$)	K_d(s^{-1})	Chi^2	R_{max}
ACE-05	6.78E-10	1.52E+06	1.03E-03	3.01E-01	12	2.15E-08	1.59E+04	3.42E-04	6.89E-02	3.5
ACE-31	2.72E-08	6.91E+04	1.88E-03	3.57E-02	10	2.39E-10	1.71E+06	4.10E-04	3.51E-02	5.2
BiTE-05	1.39E-09	8.07E+05	1.12E-03	5.91E-02	7.1	1.01E-09	1.32E+05	1.33E-04	7.42E-03	7.3
YBL-007	6.46E-10	1.47E+06	9.53E-04	1.47E-01	6.8	-	-	-	-	-
UCHT1	-	-	-	-	-	2.65E-10	1.96E+06	5.15E-04	5.69E-02	5.5

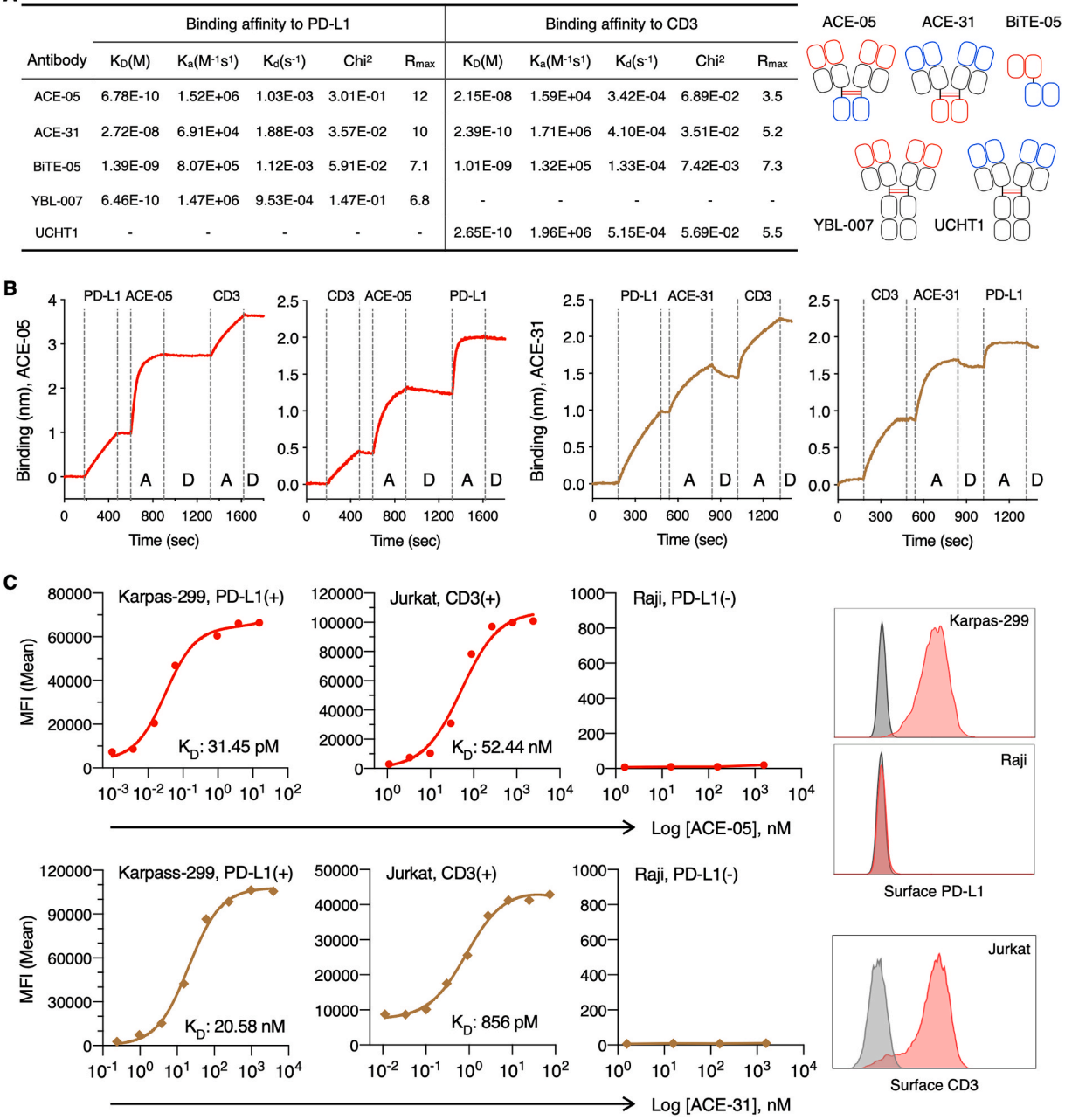

Fig. 2. Binding kinetics and concurrent binding ability of ALiCE toward PD-L1 and CD3. (A) Surface plasmon resonance (SPR) analysis for measuring the binding kinetics of ACE-05 (anti-PD-L1 Fab × anti-CD3 Fv), ACE-31 (anti-CD3 Fab × anti-PD-L1 Fv), BiTE-05 (anti-PD-L1 Fv × anti-CD3 Fv), YBL-007 (anti-PD-L1 antibody) and UCHT1 (anti-CD3 antibody) toward PD-L1 and CD3, immobilized on CM5 sensor chips. The equilibrium dissociation constant (M, K_D) was calculated as the ratio of off-rate to on-rate (K_d/K_a). Kinetic parameters were determined with the global fitting function of Biacore Insight Evaluation Software using a 1:1 binding model for monovalent ligand-analyte interactions and a 1:2 binding model for bivalent ligand-analyte interactions. Goodness of fit was assessed by evaluating Chi^2 and R_{max} values generated by fitting analyses. Red and blue ovals in the schematic diagram indicate variable domains (VH-VL) for PD-L1 and CD3 binding, respectively (right). (B) Concurrent binding of ALiCE (ACE-05 and ACE-31) toward both PD-L1 and CD3. Sensorgrams for association (A) and dissociation (D) of the indicated proteins were obtained using an Octet QKe instrument. (C) Apparent binding affinity of ALiCEs (ACE-05 or ACE-31) to PD-L1$^+$ Karpas-299 cells, PD-L1$^-$ Raji cancer cells and CD3$^+$ Jurkat T cells. Expression of PD-L1 or CD3 on the surfaces of Karpas-299 cells, Raji cancer cells or Jurkat T cells was confirmed by flow cytometry using PE-Cy7–conjugated anti-human CD274 antibody or FITC-conjugated anti-CD3 antibody, respectively (right). Karpas-299, Raji, and Jurkat T cells were treated with the indicated concentrations of ACE-05 (0.000932, 0.003729, 0.014915, 0.059662, 0.59459, 3.81, and 15.27 nM for Karpas-299; 1.56, 15.625, 156.25, and 1562 nM for Raji; 1.1, 3.3, 9.9, 29.6, 88.9, 266.7, 800, and 2400 nM for Jurkat T) or ACE-31 (0.59459, 3.81, 15.27, 61.03, 244.37, 977.5, and 3910 nM for Karpas-299; 1.56, 15.625, 156.25, and 1562 nM for Raji; 0.011, 0.033, 0.101, 0.304, 0.914, 2.743, 8.320, 24.691, and 74.074 nM for Jurkat T), and their binding was detected using an Alexa 647-conjugated anti-human Fab antibody. The equilibrium constant (K_D) was determined with Prism 8 software using "One-site specific-binding" analysis for the 1:1 binding model (stem Fv) and "Two-site total-binding" analysis for the 2:1 binding model (Fab arm).

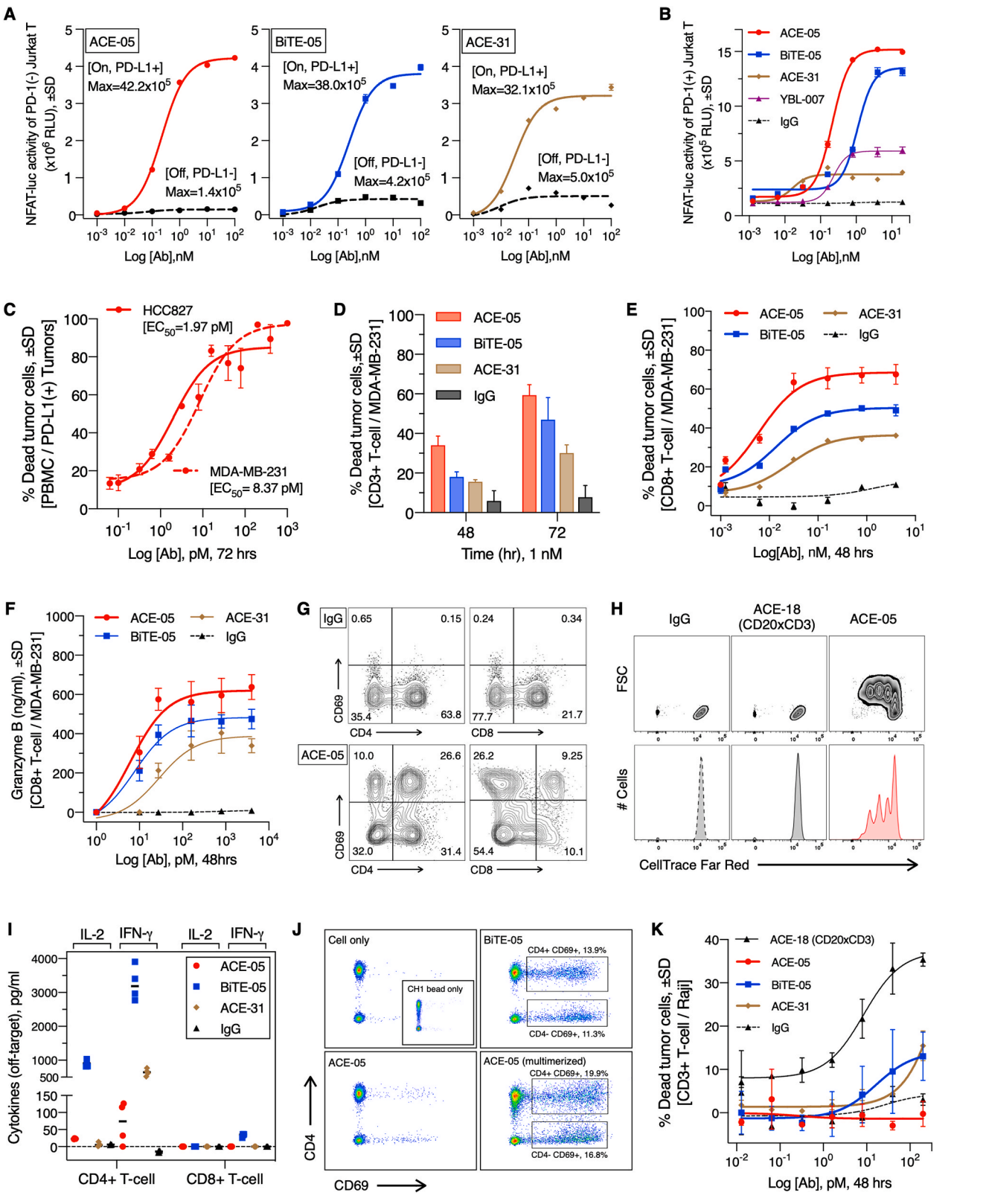

(caption on next page)

Fig. 3. ALiCE exhibits enhanced anti-tumor effects and reduced non-specific cytotoxicity in cultured cancer cells. (A) On- and off-target activation of PD-1$^-$ Jurkat T cells by ALiCE and BiTE. WT PD-L1$^-$ HEK cells or genetically engineered PD-L1$^+$ HEK cells were co-cultured with PD-1$^-$ Jurkat T cells stably expressing an NFAT-luciferase reporter gene. Cells were mixed with a T-cell engager (ACE-05, ACE-31 or BiTE-05), and PD-1$^-$ Jurkat T cell activation was assessed by measuring NFAT-luciferase reporter activity. (B) Combined effects of ALiCE on immune checkpoint inhibition and T cell redirection. Jurkat T cells stably expressing human PD-1 and an NFAT-luciferase reporter were mixed with PD-L1/aAPC$^+$ CHO–K1 cells and different concentrations (0.0064, 0.032, 0.16, 0.8, 4, 20 and 100 nM) of the indicated proteins (ACE-05, BiTE-05, ACE-31, YBL-007 or IgG), and Jurkat T-cell activation was assessed by measuring NFAT-luciferase reporter activity. (C) Concentration-dependent lysis of PD-L1$^+$ HCC827 and MDA-MB-231 cancer cells by ACE-05. PD-L1$^+$ HCC827 and MDA-MB-231 cancer cells were co-incubated with healthy donor-derived PBMCs and the indicated amounts of ACE-05 for 72 h. The percentage of dead tumor cells was determined by quantifying LDH released. E:T ratios were 25:1 for PBMC:HCC827 cells and 20:1 for PBMC:MDA-MB-231 cells. The percentage of dead tumor cells was calculated as (Experimental – Target spontaneous – Effector spontaneous)/(Target max – Target spontaneous) × 100%. Means ± SDs of triplicate determinations and calculated EC_{50} are shown. (D) Anti-tumor effects of ALiCE induced by redirection of effector cells to PD-L1$^+$ cancer cells. PD-L1$^+$ MDA-MB-231 cancer cells and CD3$^+$ T cells isolated from human PBMCs were co-cultured at an effector:target cell (E:T) ratio of 10:1 with 1 nM ACE-05, BiTE-05, ACE-31 or IgG. After incubating for 48 or 72 h, LDH released by dead tumor cells was measured by ELISA. (E) CD8$^+$ T cell cytotoxicity mediated by ACE-05. PD-L1$^+$ MDA-MB-231 tumor cells and CD8$^+$ T cells isolated from PBMCs at an E:T ratio of 5:1 were co-cultured with ACE-05, BiTE-05, ACE-31 or IgG (0.00128, 0.0064, 0.032, 0.16, 0.8 and 4 pM) for 48 h. LDH released form dead tumor cells were measured by ELISA. Mean ± SDs of triplicate determinations are shown. (F) Granzyme B released from effector CD8$^+$ T cells by bispecific T-cell engagers. CD8$^+$ T cells and PD-L1$^+$ MDA-MB-231 cancer cells were co-cultured at an E:T ratio of 5:1 together with the indicated amounts of ACE-05, BiTE-05, ACE-31 or IgG for 48 h. Granzyme B released from effector CD8$^+$ T cells was measured by ELISA. (G) On-target T cell activation by ACE-05. CellTrace-stained CD3$^+$ T cell and PD-L1$^+$ MDA-MB-231 cancer cells were co-cultivated with 1 nM ACE-05 or IgG. After 24 h incubation, T cells were labeled with APC-conjugated anti-CD4 antibody, FITC-conjugated anti-CD8 antibody, and PE-Vio 770–conjugated anti-CD69 antibody and analyzed by flow cytometry. Activated T cells were identified by analyzing CD4$^+$ CD69$^+$ and CD8$^+$ CD69$^+$ T cell subsets. (H) Stimulation of T cell expansion by ACE-05. Cell Trace Far Red-stained T cells and PD-L1$^+$ MDA-MB-231 cells were co-incubated with IgG, ACE-18 or ACE-05. After 4 days, T cell expansion was analyzed by flow cytometry. (I) Off-target cytokine release from CD4$^+$ or CD8$^+$ T cells by ALiCE. ACE-05, BiTE-05, ACE-31, or IgG (1 nM each) was directly added to CD4$^+$ or CD8$^+$ T cells isolated from human PBMCs. After a 24-h incubation, cytokines (IL-2, IFN-γ) released from CD4$^+$ or CD8$^+$ T cells were measured by ELISA. (J) Off-target T cell activation by multimeric T-cell engagers in the absence of tumor cells. CD3$^+$ T cells isolated from human PBMCs were incubated with 1 nM ACE-05, BiTE-05, or clustered ACE-05 on beads. Clustered ACE-05 was prepared by mixing 5 μl of CH1 beads with 1 nM ACE-05. After a 48-h incubation, T cells were labeled with FITC-conjugated anti-CD4 antibody and PE-Vio 770–conjugated anti-CD69 antibody and analyzed by flow cytometry. Activated T cells were identified by analyzing CD4$^+$ CD69$^+$ and CD4$^-$ CD69$^+$ T-cell subsets. (K) Non-specific killing induced by ALiCE. Raji cells (1×10^5 cells/ml) and CD3$^+$ T cells isolated from PBMCs (1×10^6 cells/ml) were co-cultured for 24 h together with ACE-05, BiTE-05, ACE-31, ACE-18 (anti-CD20 Fab × CD3 Fv), or IgG. ACE-18, which can bind to CD20$^+$ Raji cells, was used as a positive control. Cell lysis was quantified by measuring LDH release. The graph was plotted using Prism 8 software. Means ± SDs of triplicate determinations are shown.

effective T-cell activation.

We next compared the cytolytic abilities of ACE-05, ACE-31 and BiTE-05 against PD-L1$^+$ tumor cells (HCC827 or MDA-MB-231) using human effector cells (peripheral blood mononuclear cells (PBMCs) or isolated T cells). Consistent with NFAT reporter assays of PD-L1$^+$ Jurkat T cells co-cultured with engineered CHO–K1 cells, incubation of ACE-05 with effector cells (PBMCs or CD3$^+$ T cells) resulted in the most potent on-target killing activities against PD-L1$^+$ HCC827 (EC_{50} = 1.97 pM) and MDA-MB-231 (EC_{50} = 8.37 pM) cells (Fig. 3C and D, Figs. S6B–6D). Because CD8$^+$ cytotoxic T cells are often considered as the major effector cells in solid tumors, we tested whether CD8$^+$ T cells isolated from PBMC become cytotoxic upon treatment of ACE-05. Consistently, incubation of ACE-05 with CD8$^+$ T cells and PD-L1$^+$ MDA-MB-231 showed the most potent cytolytic activities and the highest level of Granzyme B secretion which lead to direct proteolysis and caspase-mediated apoptosis of target tumor cell in cooperation with perforin [31] (Fig. 3E and F). We also investigated whether ACE-05 can stimulate the activation and expansion of human effector cells in the presence of PD-L1$^+$ tumor cells. To this end, we incubated human CD3$^+$ T cells with PD-L1$^+$ MDA-MB-231 cells and 1 nM ACE-05 or IgG for 24 h, then monitored the surface expression of activation marker CD69 and CD25 [32]. The early activation marker CD69 was upregulated on both CD4$^+$ and CD8$^+$ T cells in the presence of ACE-05 and PD-L1$^+$ tumor cells, but was not upregulated by IgG (Fig. 3G). Moreover, CD25, late activation marker was also highly upregulated on CD3$^+$ T cells by ACE-05 in the presence of PD-L1$^+$ tumor cells (Fig. S6E). Activation of T cells and their subsequent differentiation to effector cells are also correlated with T-cell clustering and aggregation [33]. Therefore, we incubated CytoLight-stained human CD3$^+$ T cells with PD-L1$^+$ MDA-MB-231 cells and 1 nM ACE-05, ACE-31, BiTE-05, or IgG for 90 h, then measured cluster area. Our results clearly indicate that ACE-05 can stimulate clustering of CD3$^+$ T cells on PD-L1$^+$ tumor cells and induce T-cell activation more effectively than ACE-31 or BiTE-05 (Fig. S6F). Moreover, ACE-05 strongly induced CD3$^+$ T-cell proliferation/expansion (Fig. 3H).

Unexpectedly, however, we found that, although the on-target tumor-killing ability of ACE-05 was greater than that of BiTE-05 against both cancer cell lines (HCC827 and MDA-MB-231), the levels of released interleukin (IL)-2 and interferon (IFN)-γ in BiTE-05–treated PBMCs was even higher than that in the ACE-05–treated group (Fig. S6G). These results suggest that on-target tumor-killing activity of ACE-05 is closely associated with ACE-05's ability for T-cell redirection and immune-checkpoint inhibition rather than cytokine release from activated effector cell. To further confirm these suppositions, we generated ACE-05 variants with different binding affinities for CD3 (ACE-05 > ACE-49 > ACE-47 > ACE-56), but with the same binding affinity for PD-L1 (Fig. S7A). ACE-05, which has the highest affinity for CD3, showed the highest off-target T-cell activation in NFAT reporter assays, and off-target T-cell activation successively decreased for ACE-05 variants with decreasing binding affinity for CD3 (Fig. S7B). Surprisingly, the on-target tumor-killing ability of CD3$^+$ T cells in the presence of PD-L1$^+$ tumor cells was similar for ACE-05 and ACE-05 variants (Fig. S7C). Consistent with the previous results for uncoupling of toxic cytokines release with T cell cytolytic activity by anti-HER2/CD3 bispecific antibody [34], the cytokine release might be disconnected from T cell cytolytic activity of ACE-05, which can be mainly mediated by the secreted granzyme B and perforin. These observations collectively suggest that the ability of ALiCE to bind tumor PD-L1 for T-cell engagement and immune-checkpoint inhibition is more crucial for its anti-tumor effects, as long as ALiCE binds to CD3 even with low affinity.

To assess off-target T-cell activation by ACE-05, ACE-31 and BiTE-05, we measured secretion of the cytokines IL-2 and IFN-γ after treatment of CD4$^+$ or CD8$^+$ T cells with ACE-05, ACE-31 or BiTE-05 in the absence of PD-L1+ tumor cells. Intriguingly, only BiTE-05 strongly induced secretion of IL-2 and IFN-γ from CD4$^+$ T cells, despite the fact that the affinity of BiTE-05 for CD3 is lower than that of ACE-31 (Fig. 3I; IL-6 and TNF-α were undetected). It has been reported that clustering and/or multimerization of CD3 induced by CD3 antibody binding is more critical for T-cell activation than the CD3 binding affinity of the CD3 antibody [35]. Unlike ACE-05 and ACE-31, which are homogeneous hetero-tetrameric complexes, a gel filtration analysis indicated that the BiTE-05 preparation contained various mis-folded multimeric forms (Fig. S2C). Indeed, these multimeric components of BiTE-05 can directly activate CD4$^+$ and CD8$^+$ T cells, even without tumor cells

(Fig. 3J), possibly resulting in non-specific off-target T-cell toxicity, or cytokine-release syndrome (CRS). The PD-L1$^+$ tumor-specific T-cell cytotoxicity of ACE-05 was also confirmed by tumor-killing assays using PD-L1$^-$ Raji tumor cells with CD3$^+$ T cells isolated from PBMCs (Fig. 3K). Taken together, these findings indicate that a higher affinity of ACE-05 for tumor cells increases on-target T-cell activation, and the homogeneous hetero-tetrameric ACE-05 exhibited reduced non-specific T-cell toxicity compared with BiTE-05.

3.4. *In vivo* anti-tumor efficacy of ALiCE in a humanized mouse model

The *in vivo* anti-tumor efficacy of ALiCE was investigated in PBMC-reconstituted NCG mice engrafted with PD-L1$^+$ HCC827 tumor cells [36,37]. Briefly, PBMCs isolated from two healthy donors were implanted into female NCG mice 3 days before subcutaneous inoculation of PD-L1$^+$ HCC827 tumor cells into the right rear flank. When tumors were palpable (day 4), mice were intravenously injected with three doses of ACE-05 or BiTE-05 (0.5 mg/kg body weight), or three doses of YBL-007 or IgG (5.0 mg/kg body weight). Surprisingly, pre-established tumors had completely regressed by day 12 in 9 out of 10 ACE-05–-treated mice (Fig. 4A). We also monitored changes in body weight as an indication of side effects. BiTE-05–treated mice showed a significant loss of body weight (~20%), whereas mice treated with ACE-05 or YBL-007 did not (Fig. 4B). We speculate that body weight loss in BiTE-05–treated mice was likely attributable to a spike in cytokine release after the first administration of BiTE-05. Moreover, a pharmacokinetic analysis showed that ACE-05 had a much longer half-life than BiTE-05 in rats and cynomolgus monkeys (Fig. 4C). A dose de-escalating analysis showed that even a very low dose of ACE-05 (0.05 mg/kg body weight) resulted in complete regression of PD-L1$^+$ HCC827 tumors (Fig. 4D).

We further explored the *in vivo* T cell toxicity and anti-tumor efficacy of ACE-05 and BiTE-05 in hCD3ε transgenic (TG) mice, in which T cells have been genetically engineered to express both hCD3ε and mCD3ε. IL-2 and IFN-γ are both pleiotropic cytokines which are an important effector molecule for anti-tumor immunity through various mechanisms. However, immune related adverse effects of IL-2 and the immune-evasive function of IFN-γ have been also reported [38]. Moreover, IL-6 and TNF-α, a pro-inflammatory cytokine released from activated antigen presenting cells (APCs) such as macrophage, dendritic cells, or B cells, have been proposed as central mediators of CRS toxicity [39]. Therefore, to assess off-target T-cell toxicity, we injected a single dose of ACE-05, BiTE-05 or IgG into hCD3ε TG mice and measured the serum cytokines, IL-2, IFN-γ, IL-6 and TNF-α, every 6 h. Similar to the cytokine release observed in co-cultures of PBMCs and HCC827 cells, administration of BiTE-05 into non-tumor–bearing hCD3ε mice induced greater cytokine release, particularly IL-2, IFN-γ, and IL-6 than ACE-05, producing peak cytokine levels 6 h after administration (Fig. 4E). Moreover, BiTE-05–treated non-tumor–bearing hCD3ε mice showed severe body weight loss, whereas mice treated with ACE-05 or IgG exhibited much less body weight loss (Fig. 4F), confirming the low off-target cytotoxicity of ACE-05. Consistent with the anti-tumor efficacy of ACE-05 in PBMC-reconstituted NCG mice engrafted with PD-L1$^+$ HCC827 tumor cells, ACE-05 treatment of hCD3ε TG mice engrafted with hPD-L1$^+$ CT26 tumors effectively reduced tumor size, causing complete regression in one of six mice by day 15, without causing a significant change in body weight (Fig. 4G and Fig. S8A). We then collected tumors from each mouse at the study endpoint and analyzed tumor-infiltrating lymphocytes (TILs). Unlike tumor samples collected from YBL-007– and UCHT1-treated groups, we were only able to analyze two tumor samples from the ACE-05–treated group because the small size and weight of the remaining tumors (Fig. S8B). Interestingly, ACE-05 treatment increased the numbers of viable CD45$^+$ lymphocytes and CD3$^+$ T cells in the tumor microenvironment as compared to UCHT1 treatment (Fig. 4H and I). Moreover, ACE-05 and YBL-007 induced proliferation and expansion of CD8$^+$ T cells rather than CD4$^+$ T cells (Fig. 4J and Fig. S8C), probably due to their inhibition of PD-1 and PD-L1 interaction [40].

We also explored T-cell class I MHC immunogenicity of ACE-05-HC-VH and ACE-05-HC-VL chains using *in silico* immunogenicity prediction tools [20,21]. The immunogenicity of ACE-05-LC was not analyzed, because it is the same as the native antibody LC. We first investigated the processed peptides of ACE-05-HC-VH and ACE-05-HC-VL that could be presented on MHC class-I molecules using a percentile rank cut-off of 0.3 (Supplementary Tables 1 and 2, left side). We then determined immunogenicity scores by analyzing the collected peptide sequences using MHC-I Binding Prediction. The possible immunogenic peptides (score > 0) within ACE-05-HC-VH and ACE-05-HC-VL chains are listed in Supplementary Tables 1 and 2 (right side). Potential immunogenic peptides of ACE-05-HC-VH and ACE-05-HC-VL chains were mainly found in CDRs, FRs and CH1 within variable domains. The artificial junction that connects the hinge and second VH or VL of ACE-05 was not found to be an immunogenic epitope. Taken together, these results demonstrate that ACE-05 exhibits enhanced anti-tumor efficacy with less indiscriminate cytotoxicity through tumor-specific on-target T-cell activation and a prolonged pharmacokinetic profile, which are attributed by high-affinity binding of bivalent anti-PD-L1 Fab arms of ACE-05 to PD-L1 on tumor cells and low-affinity binding of the monovalent anti-CD3 stem Fv to CD3 on T cells.

4. Discussion

This study describes the development of a novel bispecific antibody format, ALiCE, that allows co-engagement of two distinct targets—tumor antigen and an immune receptor—thus facilitating the formation of an artificial immunological synapse between tumor and effector cells. The Fc domain of two HCs in IgG were replaced with VH or VL, whose autonomous and heterodimeric assembly enabled the introduction of a new monovalent paratope targeting T cells at the stem of ALiCE, while retaining the tumor-targeting bivalent Fab arm of IgG.

Physiologically, T cells direct their cytotoxic activity towards cells expressing MHC molecules loaded with epitopes recognized by TCRs [35]. Antibodies targeting CD3ε in association with TCRs can bypass normal TCR-MHC interactions, triggering T-cell activation [41]. However, it has been reported that several bivalent antibodies targeting CD3, including UCHT1 and OKT3, can promote cross-linking of TCR signaling complexes or induce specific conformational changes in these complex, resulting in non-specific activation of effector cells in the absence of target cells as well as inducing massive cytokine release that can cause cytokine release syndrome (CRS) or neurotoxicity [4,41]. These off-target effects and cellular toxicity have posed challenges to the development of anti-CD3 bivalent antibodies as drugs. Therefore, monovalent scFv or Fab targeting CD3 has been utilized as an alternative to reduce unspecific T-cell activation. In the current study, we found that the affinity of the monovalent stem Fv of ACE-05 (anti-PD-L1 Fab × anti-CD3 Fv) for CD3 was ~80-fold lower than that of its parent anti-CD3 bivalent antibody, UCHT1, reducing off-target cellular toxicity in cell-based reporter assays. Interestingly, among the bispecific T-cell engagers ACE-05, BiTE-05 and ACE-31, only BiTE-05 strongly induced secretion of IL-2 and IFN-γ by CD4$^+$ T cells in the absence of tumor cells, potentially resulting in off-target T-cell toxicity despite the lower affinity of BiTE-05 for CD3 compared with ACE-31 (Fig. 3I). Indeed, BiTE-05 preparations contained various multimeric forms, probably owing to its low stability (Figs. S2C and S3A), that directly activated T cells in the absence of tumor cells (Fig. 3J), demonstrating that clustering and/or multimerization of CD3 by anti-CD3 antibody binding is more critical for T-cell toxicity than the binding affinity of the anti-CD3 antibody for CD3 on T cells [35]. Moreover, treatment of human CD3ε TG tumor-free mice with BiTE-05 (anti-PD-L1 × anti-CD3) caused a spike in cytokine release after 6 h; this effect was considerably diminished in ACE-05–treated mice, despite the fact that binding affinities of ACE-05 and BiTE-05 for CD3 are comparable. These results suggest that homogeneous hetero-tetrameric ACE-05 may have fewer side effects, such as cytokine

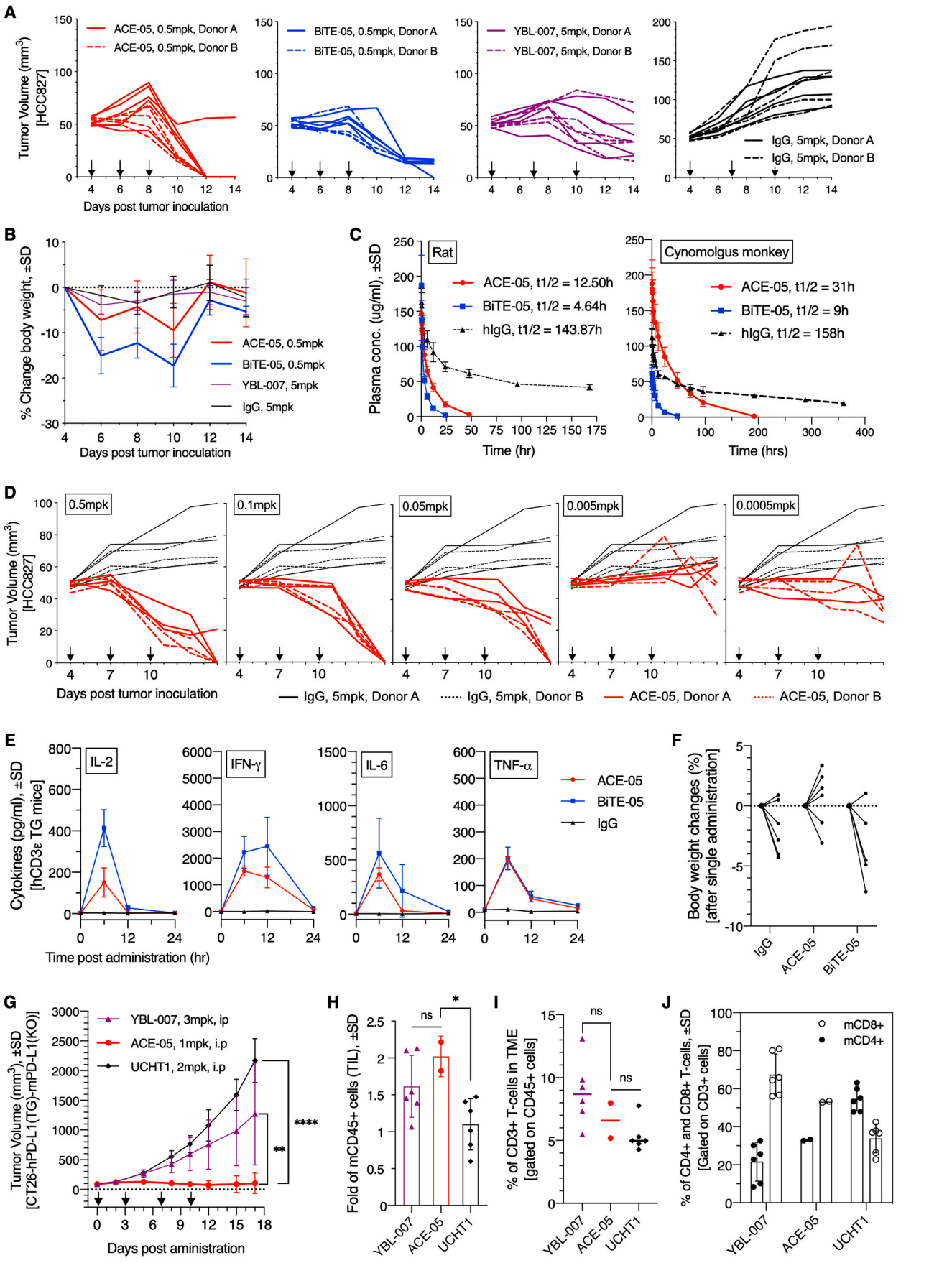

(caption on next page)

Fig. 4. *In vivo* anti-tumor efficacy of ACE-05 in a humanized mouse model. (A) Female NCG mice, aged 7–8 weeks (n = 5/group, group/donor) were intravenously injected with human PBMCs (5×10^6 cells/100 μl per mouse). Three days later, mice were inoculated subcutaneously in their right flank with HCC827 tumor cells (5×10^6 cells/mouse) in 0.1 ml PBS. When tumor volumes reached ~50 mm^3, mice were intravenously administered ACE-05 or BiTE-05 at a dose of 0.5 mg/kg every other day or with YBL-007 or IgG at a dose of 5 mg/kg every third day. On day 12, inoculated tumors had completely regressed in 9 of 10 mice treated with ACE-05. Arrows indicate times of injection. (B) Body weight changes (%) in PBMC-reconstituted mice after injection of the indicated proteins. Solid arrows indicate the times of injection of ACE-05 and BiTE-05, whereas dashed arrows indicate times of injection of YBL-007 and IgG. (C) Pharmacokinetic analysis of ALiCE in male Sprague-Dawley (SD) rats aged 6–7 weeks (n = 3/group) and male cynomolgus monkeys aged 24–29 months (n = 3/group). ACE-05, BiTE-05 or human IgG was administered intravenously to SD rats at a concentration of 10 mg/kg and to cynomolgus monkeys at a concentration of 5 mg/kg. Sera were collected from rats at 10 and 30 min; 1, 2, 4, 8 and 24 h; and 3, 5 and 9 days; and from cynomolgus monkeys at 10 and 30 min; 1, 2, 3, 6, 12 and 24 h; and 2, 3, 4, 8, 12, and 15 days. Pharmacokinetic analyses were performed using a Gyrolab xPlore automated immunoassay system; the concentrations of each sample were calculated by Gyrolab software, and $t_{1/2}$ values were determined using Phoenix WinNonlin software. (D) Anti-tumor effects of ACE-05 dose reduction. At an ACE-05 dose of 0.05 mg/kg, 4 of 6 mice showed complete regression of inoculated tumors. Arrows indicate times of injection. (E) Off-target cytokine release *in vivo*. Female non-tumor–bearing hCD3ε TG mice, aged 6–7 weeks, were injected with a single 0.5-mg/kg dose of ACE-05 or BiTE-05, or a 5-mg/kg dose of IgG, via the tail vein. Blood samples for cytokine analysis were collected from each animal at specific time points (0, 6, 12 and 24 h). The levels of various cytokines (IL-2, IFN-γ, IL-6 and TNF-α) in each collected plasma samples were measured using Cytometric Bead Array (CBA) kits. Calculated cytokine levels were plotted using GraphPad Prism 8 software. Means ± SDs of triplicate determinations are shown. (F) Body weight changes (%) in non-tumor–bearing hCD3ε mice after a single administration of T-cell engagers (ACE-05 and BiTE-05, 0.5 mg/kg; IgG, 5 mg/kg). (G–H) hCD3ε TG mice, aged 6–7 weeks, were inoculated subcutaneously in their right flank region with 5×10^5 hPD-L1-CT26 cells. Intraperitoneal (i.p.) injections of test formulations (ACE-05, 1 mg/kg; YBL-007, 3 mg/kg; and UCHT1, 2 mg/kg) were started when subcutaneous tumor volumes reached ~90 mm^3 via and were continued twice a week for 2 weeks (BIW, 4 doses total). (G) Anti-tumor efficacy of ACE-05 in hCD3ε TG mice carrying hPD-L1–expressing CT26 tumors. Arrows indicate injection times. (H–J) One week after the last injection, the percentage of live lymphocytes and T-cell subset in tumor tissues were analyzed by flow cytometry using multiple lymphocytes markers (mCD45, mCD4, mCD8, and hCD3). (H) Percentage of live $CD45^+$ tumor-infiltrating lymphocytes in the collected tumors from mice. (I) Percentage of $mCD45^+$ $hCD3^+$ T cells in the tumor microenvironment. (J) Proportion of $hCD3^+$ $mCD4^+$ and $hCD3^+$ $mCD8^+$ T cells (gated on $mCD45^+$ cells). The statistical significance was determined by one-way ANOVA with Dunnett's comparison test. *, p = 0.0199; ns, no significance.

release syndrome than BiTE-05. Although the discrepancy of cytokine release at *ex vivo* (Fig. 3I) and *in vivo* (Fig. 4E) model upon treating ACE-05 and BiTE-05 in the absence of tumor is not clear yet, the systemic increase of acute pro-inflammatory cytokine such as IL-6 and TNF-α may further induce inflammatory response of systemic effector immune cells. In fact, it has been reported that IL-6 and TNF-α has been posited as a central mediator of CRS toxicity. Therefore, IL-6R or TNF-α antagonists have been tried to manage CRS toxicity without affecting anti-tumor efficacy in patients treated with CD3 bispecific antibodies [34].

Although T cells must remain activated to efficiently eliminate tumor cells, tumor cells often contribute to the induction of immune suppression. In particular, an immune checkpoint such as the PD1/PD-L1 pathway can induce T-cell anergy and apoptosis [42], such that antibodies against PD-1 or PD-L1 have dramatic clinical effects in tumor patients. However, 70–80% of cancer patients do not spontaneously develop tumor-reactive T cells, so they do not respond to these immune-checkpoint inhibitors. Recently, anti-PD-L1 × anti-CD3 BiTE, which binds simultaneously to both PD-L1 and CD3, was shown to activate effector cells, including $CD4^+$ and $CD8^+$ T cells and natural killer T cells, which are specifically cytotoxic towards $PD\text{-}L1^+$ tumor cells [43]. Similarly, our designed ACE-05 (anti-PD-L1 Fab × anti-CD3 Fv) can bind both PD-L1 and CD3, thereby not only inhibiting PD-1/PD-L1-mediated immune suppression but also activating T cells that can kill tumor cells. The higher valency for tumor antigen binding is generally desirable, as it usually leads to increased binding avidity and greater potency of T-cell–engaging bispecific antibodies. Several "2 + 1" bispecific platforms for T cell engager, including CrossMab-Fab, IgG (kih)-ScFab, DNL-Fab_3, and DNL-Fab-ScFv have been reported [44–46]. However, these platforms either have asymmetric paratope locations or inconsistent distances between the two paratopes owing to the presence of flexible connecting linkers. The bivalent Fab domain of ALiCE is very rigid, and the disulfide bonds within its hinge create geometric constraints between C-terminal Fv and the two Fab arms. These unique structural features of ALiCE may allow it to maintain a consistent, stable immunological synapse with a distance of ~150 Å by simultaneously binding to PD-L1 on cancer cells and CD3 on T cells. Moreover, the bivalent anti-PD-L1 Fab arm of ACE-05 resulted in higher binding affinity for PD-L1 compared with that of BiTE-05, increasing contact between tumor cells and effector cells and enhancing T-cell activation and tumor-killing activity. For these reasons, the therapeutic window of ACE-05 for anti-tumor efficacy in humanized NCG mice carrying human NSCLCs can be considerable (0.05–0.5 mg/kg body weight) (Fig. 4D). More interestingly, ACE-05 significantly induces granzyme B secretion and predominantly facilitated effector $CD8^+$ T cell activation and proliferation/expansion by activation of CD3 signals and inhibition of PD-1/PD-L1-mediated immune suppression (Fig. 3E and F), thus in turn resulting in potent tumor killing. Although some tumors constitutively express PD-L1, IFN-γ and other pro-inflammatory cytokines secreted by tumor-infiltrating effector cells can trigger the expression of PD-L1 through adaptive immune resistance [47]. Therefore, ACE-05 may also be effective against tumor cells expressing low levels of PD-L1.

Pharmacokinetic profiles of antibodies are usually determined by antibody recycling through binding to neonatal FcR (FcRn) and first-pass renal filtration. In particular, drugs smaller than ~60 kDa are rapidly eliminated by glomerular filtration in the kidneys [48]. Although blinatumomab (anti-CD19 × anti-CD3 BiTE) was approved by the U.S. FDA in 2014 for the treatment of acute lymphoblastic leukemia, small-sized BiTEs (~55 kDa) that lack Fc regions have a short half-life *in vivo* and thus require continuous infusion [49]. Although ACE-05 also lacks an Fc region, its size (~140 kDa) is similar to that of IgG and much larger than BiTE; thus, it exhibits a longer half-life in the sera of rats ($t_{1/2}$ = 12.5 h) and cynomolgus monkeys ($t_{1/2}$ = 31 h) than BiTE ($t_{1/2}$ = 4.6 h in rats and 9.0 h in cynomolgus monkeys). Since the molecular weights of ACE-05 and BiTE-05 are ~140 and ~55 kDa, respectively, at a delivered dose of 0.5 mg/kg, the effective molar dose of BiTE-05 in *in vivo* anti-tumor efficacy tests was twice of ACE-05 (BiTE-05, 182 pmol; ACE-05, 80 pmol; Fig. 4A). On the other hand, because of its smaller size, BiTE-05 can penetrate into tumor tissue more efficiently than ACE-05. Given these contradictory properties, it is difficult to directly compare the *in vivo* efficacy and pharmacokinetics of ACE-05 and BiTE-05 at the same dose of administration. Furthermore, the anti-CD3 component of ACE-05 was adopted from the anti-CD3 antibody, UCHT1, which is unable to recognize CD3 in mouse and cynomolgus monkeys, limiting the ability to perform DMPK (Drug Metabolism and Pharmacokinetics) analyses of ACE-05 in non-human primate models. Mandikian et al. previously reported that, although the distribution of a bispecific antibody (anti-HER2 x anti-CD3) to the spleen and lymph nodes was correlated with CD3 affinity, a binding affinity of ~50 nM for CD3 on T cells was not sufficient to drive its distribution to lymphatic organs [50]. Most likely, ACE-05, which has a binding affinity for CD3 of 21 nM, would not localize to the secondary lymphoid system. However, a systemic pharmacokinetic analysis of a new ALiCE (anti-PD-L1 FaB × cross-reactive anti-CD3 Fv) should be performed in a non-human

primate model prior to clinical application of ALiCE. Various strategies, such as PEGylation, can also be investigated for extending the half-life of ALiCE [51].

It is known that bringing epitopes closer to the cell membrane can be beneficial for more efficient target cell killing via T-cell–engaging bispecific antibodies [52]. Moreover, the expression level of tumor antigens and their properties on cell membranes, such as mobility and distribution pattern, are significant determinants of T-cell activation and stimulation of cytokine release [48]. Therefore, the identification of novel tumor surface antigens and the selection of appropriate tumor antigens/epitopes are crucial for the development of T-cell–engaging bispecific antibodies. Because the Fab domain of any antibody can be utilized for the Fab arm of ALiCE, the ALiCE platform can be simply applied to various antibodies that target different tumor antigens and their distinct epitopes, such as CD19, EphA2 receptor tyrosine kinase, EpCAM, EGFR, melanoma-associated chondroitin sulfate proteoglycan, and CD33 [48,53]. Moreover, although the reduced binding affinity of stem Fv to CD3 compared to parental antibody was advantageous in this study, further optimization of the linker at hinge regions is also required to retain the binding affinity of parental antibody for other general applications.

5. Conclusions

In conclusion, different "2 + 1" valency and an appropriate distance between two paratopes of ALiCE for making of immunological synapse with tumor cells are properties of ALiCE that are invaluable for effective cancer therapy and avoiding high levels of cytokine release. Ultimately, the clinical applicability of the "2 + 1" ALiCE platform, including its *in vivo* immunogenicity and ability to treat hematological malignancies and solid tumors, should be further explored.

Declaration of competing interest

The authors declare the following financial interests/personal relationships which may be considered as potential competing interests: Ho Min Kim and Keehoon Jung have no competing financial interests to disclose. All other authors are employees of Y-BIOLOGICS, Inc., and, at the time of this study, owned stocks or had received stock options of Y-BIOLOGICS, Inc. as a condition of employment. Ho Min Kim and Keehoon Jung have no competing financial interests to disclose. All other authors are employees of Y-BIOLOGICS, Inc., and, at the time of this study, owned stocks or had received stock options of Y-BIOLOGICS, Inc. as a condition of employment.

Acknowledgments

This research was supported by grants from the Korea Drug Development Fund (KDDF) funded by MSIT, MOTIE and MOHW, Republic of Korea (KDDF-201803-08) and from the Institute for Basic Science, Republic of Korea (IBS-R030-C1 to H.M.K.). We thank our colleagues at Y-BIOLOGICS, Inc., especially members of the Antibody Engineering team, for their contributions to this study. We also thank Alex Kwan-Ho Chung for helpful discussions and valuable insights.

Appendix A. Supplementary data

Supplementary data to this article can be found online at https://doi.org/10.1016/j.biomaterials.2021.120760.

Data availability

The raw/processed data required to reproduce these findings cannot be shared at this time due to technical or time limitations.

Author contributions

Seil Jang: Conception and design of the ALiCE structure was by, Molecular biology and physicochemical properties were assessed by, In vitro/in vivo biological experiments were performed by, The manuscript was written and revised by. Jaeho Song: Molecular biology and physicochemical properties were assessed by. NaYoung Kim: In vitro/in vivo biological experiments were performed by. Jeonghyeon Bak: Flow cytometry analyses were performed by. Keehoon Jung: Administrative, technical, and material support was provided by. Young Woo Park: Administrative, technical, and material support was provided by. Bum-Chan Park: Overall study design and analysis of results were by. Ho Min Kim: Overall study design and analysis of results were by, The manuscript was written and revised by.

References

[1] D. Hanahan, R.A. Weinberg, Hallmarks of cancer: the next generation, Cell 144 (5) (2011) 646–674.
[2] J. Tang, L. Pearce, J. O'Donnell-Tormey, V.M. Hubbard-Lucey, Trends in the global immuno-oncology landscape, Nat. Rev. Drug Discov. 17 (11) (2018) 783–784.
[3] E. Dahlen, N. Veitonmaki, P. Norlen, Bispecific antibodies in cancer immunotherapy, Ther. Adv. Vacc. Immunother 6 (1) (2018) 3–17.
[4] D. Ellerman, Bispecific T-cell engagers: towards understanding variables influencing the in vitro potency and tumor selectivity and their modulation to enhance their efficacy and safety, Methods 154 (2019) 102–117.
[5] D.J. Zack, S.L. Morrison, W.D. Cook, W. Dackowski, M.D. Scharff, Somatically generated mouse myeloma variants synthesizing IgA half-molecules, J. Exp. Med. 154 (5) (1981) 1554–1569.
[6] M.J. Feige, J. Buchner, Principles and engineering of antibody folding and assembly, Biochim. Biophys. Acta 1844 (11) (2014) 2024–2031.
[7] A. Skerra, A. Pluckthun, Assembly of a functional immunoglobulin Fv fragment in Escherichia coli, Science 240 (4855) (1988) 1038–1041.
[8] L.L.C. Schrodinger, The PyMOL Molecular Graphics System, 2015, Version 1.8.
[9] C. Engler, R. Kandzia, S. Marillonnet, A one pot, one step, precision cloning method with high throughput capability, PloS One 3 (11) (2008), e3647.
[10] Q. Xie, G. Xinyong, C. Xianjin, W. Yayu, PEI/DNA formation affects transient gene expression in suspension Chinese hamster ovary cells via a one-step transfection process, Cytotechnology 65 (2) (2013) 263–271.
[11] J.J. Lavinder, S.B. Hari, B.J. Sullivan, T.J. Magliery, High-throughput thermal scanning: a general, rapid dye-binding thermal shift screen for protein engineering, J. Am. Chem. Soc. 131 (11) (2009) 3794–3795.
[12] M. Murphy, L. Jason-Moller, J. Bruno, Using Biacore to measure the binding kinetics of an antibody-antigen interaction, Curr Protoc. Protein Sci. Chapter 19 (2006). Unit 19 14.
[13] N.J. Wittenberg, B. Wootla, L.R. Jordan, A. Denic, A.E. Warrington, S.H. Oh, M. Rodriguez, Applications of SPR for the characterization of molecules important in the pathogenesis and treatment of neurodegenerative diseases, Expert Rev. Neurother. 14 (4) (2014) 449–463.
[14] Y. Abdiche, D. Malashock, A. Pinkerton, J. Pons, Determining kinetics and affinities of protein interactions using a parallel real-time label-free biosensor, the Octet, Anal. Biochem. 377 (2) (2008) 209–217.
[15] S.Y. Kim, J.M. Jeong, S.J. Kim, W. Seo, M.H. Kim, W.M. Choi, W. Yoo, J.H. Lee, Y. R. Shim, H.S. Yi, Y.S. Lee, H.S. Eun, B.S. Lee, K. Chun, S.J. Kang, S.C. Kim, B. Gao, G. Kunos, H.M. Kim, W.I. Jeong, Pro-inflammatory hepatic macrophages generate ROS through NADPH oxidase 2 via endocytosis of monomeric TLR4-MD2 complex, Nat. Commun. 8 (2017).
[16] A.N. Doronin, A.A. Gordeev, A.E. Kozlov, Y.A. Smirnova, M.Y. Puchkova, V. M. Ekimova, Y.I. Basovskiy, V.V. Solovyev, T-cell engagers based bioassay for evaluation of PD-1/PD-L1 inhibitors activity, Biochemistry (Mosc.) 84 (7) (2019) 711–719.
[17] L. Wang, C. Yu, Y. Yang, K. Gao, J. Wang, Development of a robust reporter gene assay to measure the bioactivity of anti-PD-1/anti-PD-L1 therapeutic antibodies, J. Pharmaceut. Biomed. Anal. 145 (2017) 447–453.
[18] P.A. Moore, W. Zhang, G.J. Rainey, S. Burke, H. Li, L. Huang, S. Gorlatov, M. C. Veri, S. Aggarwal, Y. Yang, K. Shah, L. Jin, S. Zhang, L. He, T. Zhang, V. Ciccarone, S. Koenig, E. Bonvini, S. Johnson, Application of dual affinity retargeting molecules to achieve optimal redirected T-cell killing of B-cell lymphoma, Blood 117 (17) (2011) 4542–4551.
[19] J. Roman, J. Qiu, G. Dornadula, L. Hamuro, R. Bakhtiar, T. Verch, Application of miniaturized immunoassays to discovery pharmacokinetic bioanalysis, J. Pharmacol. Toxicol. Methods 63 (3) (2011) 227–235.
[20] J.J. Calis, M. Maybeno, J.A. Greenbaum, D. Weiskopf, A.D. De Silva, A. Sette, C. Kesmir, B. Peters, Properties of MHC class I presented peptides that enhance immunogenicity, PLoS Comput. Biol. 9 (10) (2013), e1003266.
[21] M. Moutaftsi, B. Peters, V. Pasquetto, D.C. Tscharke, J. Sidney, H.H. Bui, H. Grey, A. Sette, A consensus epitope prediction approach identifies the breadth of murine T(CD8+)-cell responses to vaccinia virus, Nat. Biotechnol. 24 (7) (2006) 817–819.
[22] T. Aburatani, H. Ueda, T. Nagamune, Importance of a CDR H3 basal residue in V-H/V-L interaction of human antibodies, J. Biochem. 132 (5) (2002) 775–782.

[23] K.L. Arnett, S.C. Harrison, D.C. Wiley, Crystal structure of a human CD3-epsilon/delta dimer in complex with a UCHT1 single-chain antibody fragment, Proc. Natl. Acad. Sci. U. S. A. 101 (46) (2004) 16268–16273.
[24] H.T. Lee, J.Y. Lee, H. Lim, S.H. Lee, Y.J. Moon, H.J. Pyo, S.E. Ryu, W. Shin, Y. S. Heo, Molecular mechanism of PD-1/PD-L1 blockade via anti-PD-L1 antibodies atezolizumab and durvalumab, Sci. Rep. 7 (1) (2017) 5532.
[25] U.A. Ramagopal, W.F. Liu, S.C. Garrett-Thomson, J.B. Bonanno, Q.R. Yan, M. Srinivasan, S.C. Wong, A. Bell, S. Mankikar, V.S. Rangan, S. Deshpande, A. J. Korman, S.C. Almo, Structural basis for cancer immunotherapy by the first-in-class checkpoint inhibitor ipilimumab, Proc. Natl. Acad. Sci. USA 114 (21) (2017) E4223–E4232.
[26] M.L. Dustin, D. Depoil, New insights into the T cell synapse from single molecule techniques, Nat. Rev. Immunol. 11 (10) (2011) 672–684.
[27] D.Y. Lin, Y. Tanaka, M. Iwasaki, A.G. Gittis, H.P. Su, B. Mikami, T. Okazaki, T. Honjo, N. Minato, D.N. Garboczi, The PD-1/PD-L1 complex resembles the antigen-binding Fv domains of antibodies and T cell receptors, Proc. Natl. Acad. Sci. U. S. A. 105 (8) (2008) 3011–3016.
[28] M.L. Dustin, A.K. Chakraborty, A.S. Shaw, Understanding the structure and function of the immunological synapse, Cold Spring Harb. Perspect. Biol. 2 (10) (2010) a002311.
[29] S. Offner, R. Hofmeister, A. Romaniuk, P. Kufer, P.A. Baeuerle, Induction of regular cytolytic T cell synapses by bispecific single-chain antibody constructs on MHC class I-negative tumor cells, Mol. Immunol. 43 (6) (2006) 763–771.
[30] Z.J.J. Cheng, N. Karassina, J. Grailer, J. Hartnett, F. Fan, M. Cong, Novel PD-1 blockade bioassay to assess therapeutic antibodies in PD-1 and PD-L1 immunotherapy programs, Canc. Res. 75 (2015).
[31] S.P. Cullen, M. Brunet, S.J. Martin, Granzymes in cancer and immunity, Cell Death Differ. 17 (4) (2010) 616–623.
[32] C. Haas, E. Krinner, K. Brischwein, P. Hoffmann, R. Lutterbuse, B. Schlereth, P. Kufer, P.A. Baeuerle, Mode of cytotoxic action of T cell-engaging BiTE antibody MT110, Immunobiology 214 (6) (2009) 441–453.
[33] J. Zhou, M.T. Bethune, N. Malkova, A.M. Sutherland, B. Comin-Anduix, Y. Su, D. Baltimore, A. Ribas, J.R. Heath, A kinetic investigation of interacting, stimulated T cells identifies conditions for rapid functional enhancement, minimal phenotype differentiation, and improved adoptive cell transfer tumor eradication, PloS One 13 (1) (2018), e0191634.
[34] J. Li, R. Piskol, R. Ybarra, Y.J. Chen, J. Li, D. Slaga, M. Hristopoulos, R. Clark, Z. Modrusan, K. Totpal, M.R. Junttila, T.T. Junttila, CD3 bispecific antibody-induced cytokine release is dispensable for cytotoxic T cell activity, Sci. Transl. Med. 11 (508) (2019).
[35] S. Minguet, M. Swamy, B. Alarcon, I.F. Luescher, W.W.A. Schamel, Full activation of the T cell receptor requires both clustering and conformational changes at CD3, Immunity 26 (1) (2007) 43–54.
[36] O. Ueda, N.A. Wada, Y. Kinoshita, H. Hino, M. Kakefuda, T. Ito, E. Fujii, M. Noguchi, K. Sato, M. Morita, H. Tateishi, K. Matsumoto, C. Goto, Y. Kawase, A. Kato, K. Hattori, J. Nezu, T. Ishiguro, K.I. Jishage, Entire CD3epsilon, delta, and gamma humanized mouse to evaluate human CD3-mediated therapeutics, Sci. Rep. 7 (2017) 45839.
[37] P. De La Rochere, S. Guil-Luna, D. Decaudin, G. Azar, S.S. Sidhu, E. Piaggio, Humanized mice for the study of immuno-oncology, Trends Immunol. 39 (9) (2018) 748–763.
[38] P. Berraondo, M.F. Sanmamed, M.C. Ochoa, I. Etxeberria, M.A. Aznar, J.L. Perez-Gracia, M.E. Rodriguez-Ruiz, M. Ponz-Sarvise, E. Castanon, I. Melero, Cytokines in clinical cancer immunotherapy, Br. J. Canc. 120 (1) (2019) 6–15.
[39] A. Shimabukuro-Vornhagen, P. Godel, M. Subklewe, H.J. Stemmler, H.A. Schlosser, M. Schlaak, M. Kochanek, B. Boll, M.S. von Bergwelt-Baildon, Cytokine release syndrome, J. Immunother Canc. 6 (1) (2018) 56.
[40] G. Beyrend, E. van der Gracht, A. Yilmaz, S. van Duikeren, M. Camps, T. Hollt, A. Vilanova, V. van Unen, F. Koning, N. de Miranda, R. Arens, F. Ossendorp, PD-L1 blockade engages tumor-infiltrating lymphocytes to co-express targetable activating and inhibitory receptors, J. Immunother Canc. 7 (1) (2019) 217.
[41] C. Kuhn, H.L. Weiner, Therapeutic anti-CD3 monoclonal antibodies: from bench to bedside, Immunotherapy 8 (8) (2016) 889–906.
[42] L. Chen, D.B. Flies, Molecular mechanisms of T cell co-stimulation and co-inhibition, Nat. Rev. Immunol. 13 (4) (2013) 227–242.
[43] L.A. Horn, N.G. Ciavattone, R. Atkinson, N. Woldergerima, J. Wolf, V.K. Clements, P. Sinha, M. Poudel, S. Ostrand-Rosenberg, CD3xPDL1 bi-specific T cell engager (BiTE) simultaneously activates T cells and NKT cells, kills PDL1(+) tumor cells, and extends the survival of tumor-bearing humanized mice, Oncotarget 8 (35) (2017) 57964–57980.
[44] S. Dickopf, M.E. Lauer, P. Ringler, C. Spick, P. Kern, U. Brinkmann, Highly flexible, IgG-shaped, trivalent antibodies effectively target tumor cells and induce T cell-mediated killing, Biol. Chem. 400 (3) (2019) 343–350.
[45] C. Klein, W. Schaefer, J.T. Regula, The use of CrossMAb technology for the generation of bi- and multispecific antibodies, mAbs 8 (6) (2016) 1010–1020.
[46] D.L. Rossi, E.A. Rossi, T.M. Cardillo, D.M. Goldenberg, C.H. Chang, A new class of bispecific antibodies to redirect T cells for cancer immunotherapy, mAbs 6 (2) (2014) 381–391.
[47] A. Ribas, Adaptive immune resistance: how cancer protects from immune attack, Canc. Discov. 5 (9) (2015) 915–919.
[48] Z. Wu, N.V. Cheung, T cell engaging bispecific antibody (T-BsAb): from technology to therapeutics, Pharmacol. Ther. 182 (2018) 161–175.
[49] H. Kantarjian, A. Stein, N. Gokbuget, A.K. Fielding, A.C. Schuh, J.M. Ribera, A. Wei, H. Dombret, R. Foa, R. Bassan, O. Arslan, M.A. Sanz, J. Bergeron, F. Demirkan, E. Lech-Maranda, A. Rambaldi, X. Thomas, H.A. Horst, M. Bruggemann, W. Klapper, B.L. Wood, A. Fleishman, D. Nagorsen, C. Holland, Z. Zimmerman, M.S. Topp, Blinatumomab versus chemotherapy for advanced acute lymphoblastic leukemia, N. Engl. J. Med. 376 (9) (2017) 836–847.
[50] D. Mandikian, N. Takahashi, A.A. Lo, J. Li, J. Eastham-Anderson, D. Slaga, J. Ho, M. Hristopoulos, R. Clark, K. Totpal, K. Lin, S.B. Joseph, M.S. Dennis, S. Prabhu, T. T. Junttila, C.A. Boswell, Relative target affinities of T-cell-dependent bispecific antibodies determine biodistribution in a solid tumor mouse model, Mol. Canc. Therapeut. 17 (4) (2018) 776–785.
[51] R.E. Kontermann, Strategies for extended serum half-life of protein therapeutics, Curr. Opin. Biotechnol. 22 (6) (2011) 868–876.
[52] C. Bluemel, S. Hausmann, P. Fluhr, M. Sriskandarajah, W.B. Stallcup, P. A. Baeuerle, P. Kufer, Epitope distance to the target cell membrane and antigen size determine the potency of T cell-mediated lysis by BiTE antibodies specific for a large melanoma surface antigen, Cancer Immunol. Immunother. 59 (8) (2010) 1197–1209.
[53] J.K. Lee, N.J. Bangayan, T. Chai, B.A. Smith, T.E. Pariva, S. Yun, A. Vashisht, Q. Zhang, J.W. Park, E. Corey, J. Huang, T.G. Graeber, J. Wohlschlegel, O.N. Witte, Systemic surfaceome profiling identifies target antigens for immune-based therapy in subtypes of advanced prostate cancer, Proc. Natl. Acad. Sci. U. S. A. 115 (19) (2018) E4473–E4482.